Gondwana Research 25 (2014) 1272–1286

Contents lists available at ScienceDirect

Gondwana Research

journal homepage: www.elsevier.com/locate/gr

The Mejillonia suspect terrane (Northern Chile): Late Triassic fast burial and metamorphism of sediments in a magmatic arc environment extending into the Early Jurassic

C. Casquet [a,*], F. Hervé [b,c], R.J. Pankhurst [d], E. Baldo [e], M. Calderón [f], C.M. Fanning [g], C.W. Rapela [h], J. Dahlquist [e]

[a] Departamento de Petrología y Geoquímica, Universidad Complutense — Instituto de Geociencias (UCM, CSIC), 28040 Madrid, Spain
[b] Departamento de Geología, Universidad de Chile, Plaza Ercilla 803, Santiago, Chile
[c] Escuela de Ciencias de la Tierra, Universidad Andres Bello, Sazie 2315, Santiago, Chile
[d] Visiting Research Associate, British Geological Survey, Keyworth, Nottingham NG12 5GG, United Kingdom
[e] CICTERRA-CONICET-UNC, Av. Vélez Sarsfield 1611, Pab. Geol., X5016CGA Córdoba, Argentina
[f] Servicio Nacional de Geología y Minería, Santa Maria 0104, Santiago, Chile
[g] Research School of Earth Sciences, The Australian National University, Canberra, ACT 0200, Australia
[h] Centro de Investigaciones Geológicas (CONICET-UNLP), 1900 La Plata, Argentina

ARTICLE INFO

Article history:
Received 14 March 2013
Received in revised form 7 May 2013
Accepted 14 May 2013
Available online 10 June 2013

Handling Editor: R.D. Nance

Keywords:
Mejillonia terrane
U–Pb SHRIMP zircon geochronology
Pre-Andean continental margin
Late Triassic subduction
Early Jurassic magmatic arc

ABSTRACT

The Mejillonia terrane, named after the Mejillones Peninsula (northern Chile), has been traditionally considered an early Paleozoic block of metamorphic and igneous rocks displaced along the northern Andean margin in the Mesozoic. However, U–Pb SHRIMP zircon dating of metasedimentary and igneous rocks shows that the sedimentary protoliths were Triassic, and that metamorphism and magmatism took place in the Late Triassic (Norian). Field evidence combined with zircon dating (detrital and metamorphic) further suggests that the sedimentary protoliths were buried, deformed (foliated and folded) and metamorphosed very rapidly, probably within few million years, at ca. 210 Ma. The metasedimentary wedge was then uplifted and intruded by a late arc-related tonalite body (Morro Mejillones) at 208 ± 2 Ma, only a short time after the peak of metamorphism. The Mejillones metamorphic and igneous basement represents an accretionary wedge or marginal basin that underwent contractional deformation and metamorphism at the end of a Late Permian to Late Triassic anorogenic episode that is well known in Chile and Argentina. Renewal of subduction along the pre-Andean continental margin in the Late Triassic and the development of new subduction-related magmatism are probably represented by the Early Jurassic Bólfin–Punta Tetas magmatic arc in the southern part of the peninsula, for which an age of 184 ± 1 Ma was determined. We suggest retaining the classification of Mejillonia as a tectonostratigraphic terrane, albeit in this new context.

1. Introduction

Active continental margins of Andean or Cordilleran type are accretionary orogens in the sense of Cawood et al. (2003, 2009), where a complex interplay occurs between accretionary processes *s.l.* and tectonic erosion along the subduction zone (e.g., Stern, 2011). Accretion embraces, on the one hand, subduction-related, mantle-derived, arc magmatism that contributes to the long-term growth of the continental crust and, on the other hand, the construction of accretionary wedges along the active margin front and the amalgamation of suspect terranes (for a review of terrane nomenclature see Gibbons, 1994). The latter are typically either displaced along the margin as a result of oblique subduction (transcurrent terranes), or are exotic to it (e.g., buoyant oceanic plateaux, ridges, or continental blocks). Because of its contribution to the overall growth of the active continental margin and its importance to understanding the geodynamic evolution of the orogen, a suspect terrane must be thoroughly surveyed before its identity is proven. Techniques such as SHRIMP U–Pb dating of detrital zircons in rocks with sedimentary protoliths have proved particularly useful in this regard, especially in cases where the suspect terrane is metamorphic and chronostratigraphy is obscured by deformation and recrystallization.

The proto-Andean margin of the supercontinent Gondwana in southern South America is universally interpreted as resulting from terrane accretion. Here a collage of allochthonous terranes, some allegedly exotic, has been widely accepted since the seminal contribution of Ramos (1988). These terranes were accreted to the proto-Andean margin throughout the Paleozoic and are now exposed in the basement of the Andes and in the Andean foreland in Chile and Argentina. Moreover, terrane accretion continued along the Andean

* Corresponding author. Tel.: +34 913944908; fax: +34 915442535.
E-mail address: casquet@geo.ucm.es (C. Casquet).

1342-937X/$ – see front matter
http://dx.doi.org/10.1016/j.gr.2013.05.016

margin in the early Mesozoic, exemplified by the metamorphic and plutonic terrane that constitutes the elongated Mejillones Peninsula north of Antofagasta (Fig. 1). This was first considered a terrane by Ramos (1988; Fig. 1) and allegedly docked to the Chilean margin in Jurassic time (Damm et al., 1990), probably through protracted sinistral strike-slip movements along the Atacama fault system that continued into the Middle Cretaceous (Brown et al., 1993; Bahlburg and Hervé, 1997).

The concept of the Mejillonia terrane was first based on the idea that it contains anomalously old rocks for its situation on the Andean margin. Whereas the basement of coastal Chile elsewhere at these latitudes is represented by low-grade metasedimentary rocks of probable Devonian age, several authors using a variety of geochronological methods (see details below) have claimed ages of ca. 500 Ma for igneous and metamorphic rocks from the Mejillones Peninsula (Damm et al., 1990). Significant in this regard is the fact that Cambrian plutonism and metamorphism are typical of the collisional Pampean orogeny in Argentina (e.g., Rapela et al., 1998) some 700 km east of the Pacific coast. This orogeny has been recently considered a segment of a longer mainland orogenic belt extending northward into Paraguay and Brazil along the eastern margin of the Proterozoic Amazonia craton (the Paraguay and Araguaia mobile belts). Since this is far removed from

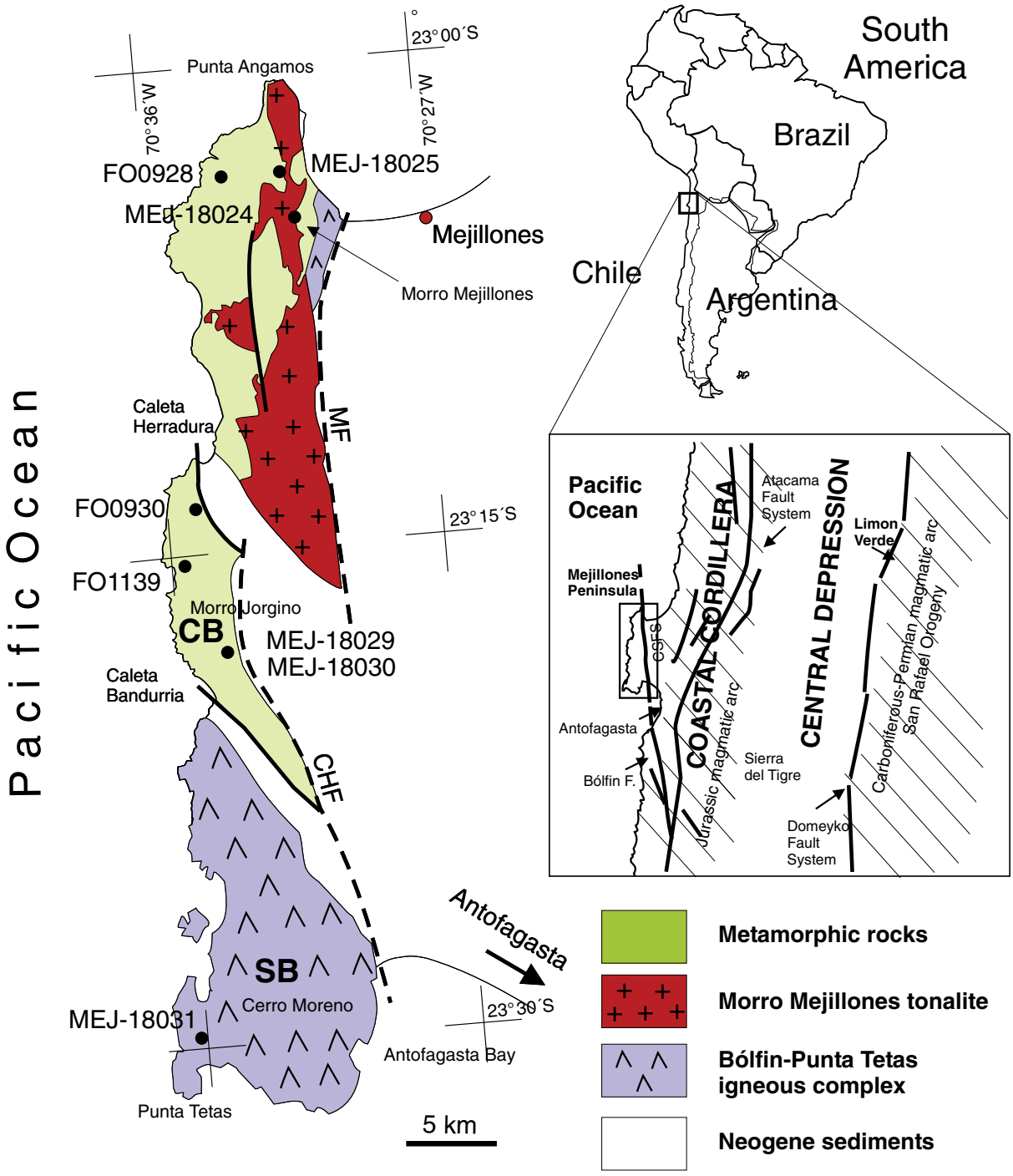

Fig. 1. Geological sketch map of the Mejillones Peninsula showing location of samples collected for SHRIMP dating. Insets show location of the peninsula in South America and in northern Chile, including the region between the coast and the High Andes. NB: northern block; CB: central block; SB: southern block. MF: Mejillones fault; CHF: Caleta Herradura fault (Cortés et al., 2008).

the Pacific coast (Casquet et al., 2012), Cambrian metamorphic rocks would not be expected west of the Pampean belt. The Mejillonia terrane consequently poses an intriguing problem with respect to the geography of the Cambrian orogeny that led to the final amalgamation of SW Gondwana (Casquet et al., 2012 and references therein).

The aim of this paper is to present new geochronological data on metamorphic and intrusive rocks of the Mejillones peninsula, obtained by SHRIMP analysis of zircons (a method not previously employed on these rocks) in order to constrain their geological and geodynamic significances.

2. Geological setting

The Coastal Cordillera of northern Chile is mainly composed of Mesozoic volcanic and plutonic rocks, which testify to the existence since Jurassic times of a magmatic arc related to east-directed subduction. Deep parts of the Jurassic magmatic arc are exposed south of Antofagasta (e.g., Bólfin Formation) and in the Mejillones Peninsula (Punta Tetas) (Fig. 1).

The Mejillones Peninsula is the largest along the North Chilean coast. It is formed of igneous and metamorphic rocks that constitute a N–S elongate massif, separated from the mainland by a low area of Neogene marine sediments that are in fault contact with the igneous and metamorphic rocks (Figs. 1 and 2). The peninsula consists of three geologically contrasting blocks (Baeza, 1984) resulting from Cenozoic extensional uplift along normal faults (horst and graben structures) (Niemeyer et al., 1996; Hartley et al., 2000) (Figs. 1 and 2). According to Baeza (1984), the northern block is formed of metapelitic rocks that exhibit mineral zonation – biotite, andalusite and sillimanite zones – related to the plutonic body of Morro Mejillones. The central Morro Jorgino block is composed of amphibolites and metapelites with a garnet, kyanite, sillimanite mineral zonation (i.e., a Barrovian-type metamorphism), whereas the southern Cerro Moreno block is composed of dioritic to gabbroic plutons of the Bólfin–Punta Tetas complex.

The Morro Mejillones pluton is an elongate N–S body consisting of coarse-grained biotite–hornblende tonalite, with igneous contacts discordant to the structural trend of the host rocks, and with many apophyses. The host rocks are gneisses and schists with a few metapsammitic layers, showing two phases of foliation and folding. S_0–S_1 is a compositional banding represented by alternating thicker quartz-rich and thinner biotite-rich layers. Folds are isoclinal and east-vergent, and near the axial zone show a foliation (S_2) that overprints S_0–S_1. An intersection lineation is common. Foliations and folding developed before pluton emplacement. The pluton does not extend into the central block, where the rocks are again banded gneisses and schists with deformed quartz veins, and amphibolites and garnet leucogranite sheets concordant or slightly discordant to the external foliation (Fig. 3). The southern block consists mainly of intermediate to basic plutonic rocks with an earlier, probably primary, foliation/lineation and superimposed mylonitization that varies from weak to strong.

The inland Paleozoic rocks of this region have been considered to form part of an accretionary prism, which developed mainly from Devonian through to Permian times (e.g., Bahlburg et al., 2009). These units are mainly composed of low-grade metamorphic rocks with predominant turbiditic protoliths, and scarce basic rocks and limestones. The higher metamorphic grade of the rocks of Mejillones Peninsula, and of those of the Limon Verde metamorphic complex east of the Atacama fault system at this latitude (Fig. 1), has been an obstacle for their consideration as an integral part of the accretionary prism. The Limon Verde rocks have been considered to belong to an intercontinental mobile belt (Lucassen et al., 2000), and the Mejillones metamorphic rocks to a tectono-stratigraphic terrane. However, Tomlinson et al. (2012) have argued, by geological analogy with the Laramide orogeny, that the Limon Verde metamorphic rocks are typical of accretionary complexes and that they record flat-slab subduction during the early to middle-Permian San Rafael phase of the Gondwanide orogeny (Fig. 1). Hervé and Mpodozis (1990), in a survey of the previously suggested terranes on the western margin of Gondwana, refer to the Mejillonia terrane as one whose age and timing of docking to Gondwana are unknown.

The basement rocks of the Mejillones Peninsula have been subjected to extensive previous geochronological study, albeit mostly in the last decades of the twentieth century. Initially, Diaz et al. (1985) presented Rb–Sr whole rock (WR) data for samples of andalusite-zone schists at Punta Angamos in the northern block, which were claimed to give a reference isochron of 530 Ma. Damm et al. (1990) obtained an imprecise Sm–Nd WR age of 521 ± 55 Ma for orthoamphibolite from a central outcrop (Morro Jorgino), and Lucassen et al. (2000) obtained an age of 525 ± 10 Ma from a Sm–Nd mineral isochron from a Morro Jorgino garnet amphibolite. These Early Paleozoic (ca. 500 Ma) ages served as the basis for interpreting the Mejillones Peninsula as an old terrane accreted to the Andean margin in the Jurassic (Damm et al., 1990; Bahlburg and Hervé, 1997).

Jurassic ages of ca. 190 Ma have been recorded from igneous rocks of the Bólfin–Punta Tetas complex in the southern block (Cerro Moreno) (Damm et al., 1986; reported by Cortés et al., 2007). In addition, K–Ar ages on muscovite, biotite and amphibole from the metamorphic and

Fig. 2. View of the Mejillones relief from the north. Uplifted basement blocks (horsts) are bounded by normal fault scarps and are topped by marine terraces. Neogene marine sediments fill the depression (graben) in the foreground.

Fig. 3. Outcrop view of garnet-bearing leucogranite MEJ-18029. For explanation see text.

igneous rocks (Basei et al., 1996; Diaz et al., 1985; Lucassen et al., 2000) generally range from 140 to 190 Ma, pointing to thermal effects throughout the Jurassic that are probably related to emplacement of the Bólfin–Punta Tetas pluton.

Hervé et al. (2010) obtained detrital zircon U–Pb SHRIMP age patterns for two low-grade metasedimentary rocks relevant to the current work: FO0928 from the Mejillones Peninsula (full data are presented for the first time here) and an amphibolite facies rock from the Limón Verde complex. The detrital age pattern of FO0928 shows mainly Early Paleozoic ages and a significant number is in the range 1000–1200 Ma. In contrast, the Limon Verde mica schist displays predominant Early Permian detrital zircons that point to sedimentation only shortly before its subsequent history of high-grade metamorphism in the Middle to Late Permian (San Rafael orogeny) and exhumation during the Triassic. This suggests that the two terranes underwent different geological histories and were simply juxtaposed along the Atacama fault system.

3. Sampling and analytical methods

Samples of metasedimentary and igneous rocks were collected at locations throughout the Mejillones Peninsula, of which eight were selected for SHRIMP U–Pb zircon dating. Sample locations are shown in Fig. 1. Coordinates and abbreviated mineralogy of the analysed samples are shown in Table 1. Notably, two samples (MEJ-18029 and MEJ-18030) were collected near the sampling locality of Lucassen et al. (2000).

3.1. Sample description

3.1.1. Metasedimentary rock samples

MEJ-18025 is a banded gneiss interbedded with grey metapsammitic beds and discordantly intruded by apophyses of the Morro Mejillones pluton. The banding reflects alternation of thin biotite-rich and thicker quartz-rich layers. This foliation (S_0–S_1) is folded: F_2 folds are a few cm to several metres in amplitude and are accompanied by development of an axial planar foliation (S_2) due to new growth of biotite and sillimanite. Mineral composition is quartz, biotite, plagioclase, K-feldspar, muscovite, sillimanite (fibrolite), andalusite and minor graphite, ore minerals and zircon. Andalusite is found as randomly orientated porphyroblasts, probably resulting from a late contact metamorphic overprint. Sillimanite and K-feldspar suggest that the rock reached high-grade metamorphic conditions during F_2.

FO0928 is a mica schist in the northern block with a cm-spaced crenulation cleavage S_2, axial planar to open folds and numerous small folds in rootless quartz veins. The rocks are intruded by cross-cutting decimetric tabular granitic bodies, probably apophyses of the nearby Morro Mejillones pluton. The rock contains oriented biotite and white mica as layers alternating with quartz richer bands.

MEJ-18030 is a banded biotite gneiss in the central block (Morro Jorgino) intercalated with amphibolite and leucogranite sheets. Its mineral composition is plagioclase, biotite and quartz with accessory zircon and apatite, and minor retrograde chlorite. The plagioclase texture is polygonal granoblastic, suggesting annealing of the rocks after deformation.

FO0930 is a banded schist on the northeastern slope of Morro Jorgino, with frequent decimetric, rootless, isoclinal folds in quartz veins. The rock is well foliated and consists of quartz, plagioclase, biotite, and white mica, with ilmenite, zircon and apatite as accessory minerals.

FO1139 is a banded schist in the central block consisting of coarse quartz bands and lenses separated by thinner biotite-rich layers, as in MEJ-18025. The biotite-rich layers contain abundant poikilitic plagioclase crystals, with unorientated biotite and quartz inclusions. Garnets are present as large equant porphyroblasts and as elongated crystals parallel to the banding of the rock, both with irregular margins. They contain quartz and opaque mineral inclusions. Opaque minerals including monazite are intergrown with biotite in some bands. The biotite has numerous zircon inclusions with dark haloes. White mica and chlorite are accessory.

3.1.2. Igneous rock samples

MEJ-18024 from Morro Mejillones is a coarse-grained tonalite with hornblende, biotite, plagioclase, K-feldspar (<5%), quartz, and titanite, ore minerals, apatite, and zircon as accessories. Secondary minerals are chlorite, epidote and sericite. No evidence for subsolidus strain is recognized.

MEJ-18029, from the same locality as MEJ-18030 on Morro Jorgino, sampled a leucogranite body almost concordant with the foliation of the host banded gneiss (Fig. 3). The leucogranite contains scattered garnet, and a little biotite, the latter showing a preferred orientation roughly parallel to the contacts, i.e., a continuous foliation. The mineral composition is quartz, microcline, plagioclase, biotite and muscovite with garnet, zircon, monazite, apatite and ore minerals as accessories. Secondary minerals are chlorite, calcite, epidote, sericite and ore minerals. No textures indicative of significant subsolidus strain are recognized.

MEJ-18031 from near Cerro Moreno in the southern block is a mylonitic hornblende–biotite quartz–diorite of the Bólfin–Punta Tetas intrusive complex. The rock consists of hornblende, plagioclase, quartz, biotite and relict clinopyroxene with accessory zircon, apatite and epidote. A mylonitic foliation is well developed with porphyroclasts of plagioclase and hornblende wrapped in a foliated groundmass of recrystallized fine-grained biotite, hornblende, plagioclase and quartz.

3.2. Analytical methods

U–Pb analyses were performed using SHRIMP RG at the Research School of Earth Sciences, The Australian National University, Canberra. Zircon fragments were mounted in epoxy together with chips of the Temora standard zircon, ground approximately half-way through and polished. Reflected and transmitted light photomicrographs, and cathodo-luminescence (CL) SEM images, were used to decipher the internal structures of the sectioned grains and to target specific areas within the zircons. The number of areas analysed per sample ranged from 25 to 60 and 20 to 30 in metasedimentary and igneous rocks respectively. The number of grains analysed for provenance was small in some metasedimentary samples. Reliable evidence was however

Table 1
Samples selected for U–Pb SHRIMP zircon dating.

Block	Sample	Coordinates	Rock type
Northern	MEJ-18024	23°05′46.1″–70°30′54.5″	Hornblende–biotite tonalite (Morro de Mejillones pluton)
Northern	MEJ-18025	23°04′24.2″–70°31′11.1″	Banded sillimanite–andalusite–biotite gneiss
Northern	FO0928	23°03′50.4″–70°32′31.2″	Biotite–schist
Central	MEJ-18029	23°18′14.0″–70°34′28.9″	Garnet-bearing leucogranite
Central	MEJ-18030	23°18′14.0″–70°34′28.9″	Banded biotite–gneiss
Central	FO0930	23°14′07.2″–70°34′45.3″	Banded biotite–gneiss
Central	FO1139	23°15′35.2″–70°35′26.5″	Banded garnet–biotite gneiss
Southern	MEJ-18031	23°29′33.6″–70°36′37.9″	Mylonitic quartz–diorite (Bólfin–Punta Tetas igneous complex)

obtained to constrain the age of the protoliths and that of metamorphic processes. The data were reduced in a manner similar to that described by Williams (1998, and references therein), using the SQUID Excel macro of Ludwig (2001). U–Pb data for the metasedimentary samples are given in Table 2 and for the igneous samples in Table 3. Partial probability plots of detrital zircon ages (showing ages back to 700 Ma) are shown in Fig. 4 and described below.

4. Analytical results

4.1. Metasedimentary rocks

The majority of zircons separated from MEJ-18025 are elongated grains with simple igneous concentric zonation, sometimes with high-U and developed on older cores, although a few are rounded grains with complex or "soccer-ball" zoning. Unmeasurably thin metamorphic rims exist on most grains. In reflected light all grains have pitted surfaces consistent with surface transport and hence a detrital origin. The SHRIMP analyses (n = 30) show mostly normal igneous Th/U ratios of 0.25–1.5. The U–Pb ages range from ca. 210 Ma to 1700 Ma. A peak at ca. 210 Ma is defined by analyses of three simple concentrically zoned igneous grains (U ca. 200–250, Th ca. 100 ppm). We see no reason to suspect that these either grew in situ at this time (in which case they would probably have much higher U and lower Th contents) or that, given their consistency, they crystallized much earlier and were subject to Pb-loss at 210 Ma; they are therefore assumed to date the age of a provenance component. Other reasonably well-defined peaks occur at ca. 275, 340, 510, 545, 625, 1045 and 1650 Ma (Fig. 4), suggesting that zircons were ultimately derived from a complex continental source. From the age of the youngest detrital zircons, the sedimentary protolith cannot have been older than Late Triassic (Norian).

FO0928 has a zircon detrital pattern with a predominant Early to Middle Ordovician population between 465 and 495 Ma (corresponding to the Famatinian orogeny) and a minor Cambrian peak at 515 Ma (Fig. 4), as well as some Proterozoic ages (a significant number of grains in the range 800–1400 Ma, and single grain ages at 1.7, 1.9 and 2.6 Ga). One apparent age of 44 Ma was rejected due to an extremely high common Pb content, as were four other ages. Two Jurassic ages were discounted on the basis of geological evidence (see below). The youngest reliable ages in this sample are Carboniferous.

MEJ-18030 contains zircons with a wide variety of morphologies revealed by cathodo-luminescence imaging, with zoned or unzoned cores often overgrown by later zircon. One large euhedral grain gave an anomalous age of 58 Ma and was discounted as a potential contaminant. The remaining 42 ages range between ca. 205 Ma and 2700 Ma, with many apparent peaks, of which the best-defined are at ca. 255, 290–320, 355, 480, 610 and 1120 Ma (Fig. 4). Most grains appear to be simple igneous zircons, but some show very thin metamorphic overgrowths (e.g., # 16.1, with the youngest age at 205 Ma and # 6 at 500 Ma). The maximum age of sedimentation of the protolith is best assessed as ca. 255 Ma (based on three grains). The detrital zircon pattern of this Morro Jorgino gneiss is essentially very similar to that of the Punta Angamos gneiss (MEJ-18025), except that the latter has a higher proportion of Mesoproterozoic grains at ca. 1.0–1.3 Ma and at 1.6–1.7 Ga.

FO0930 has three grains that gave Cretaceous (# 31.1) or Jurassic (# 1.1 and 7.1) ages, two of which could be rejected for analytical reasons (high common Pb contents), although the geological situation suggests that they do not record primary crystallization (see below). The youngest reliable age seems to be ca. 220 Ma (Table 2). The main part of the detrital zircon pattern is otherwise very similar to that of FO0928 in the northern block, with a predominant Early to Middle Ordovician population and a minor Cambrian peak (in this case ca. 550 Ma). The older components are mostly 800–1300 Ma, with one grain dated as 2.0 Ga.

FO1139 contains a complex, heterogeneous population of zircons. They range from equant to elongate subhedral grains, a few with pyramidal terminations; most have mottled surfaces and overgrowths that can be seen under transmitted light. The CL images reveal the true complexity of the internal structure. The mottled rims range from thin dark oscillatory-zoned components to broader areas with a uniformly grey CL response. For the current study 25 areas were analysed on 15 zircon grains. In general those areas analysed as inherited cores yield older $^{206}Pb/^{238}U$ ages, ranging back to ~1170 Ma, but most are Palaeozoic to Triassic (240, 290, 450, 530 Ma) although the small number of analyses may not be fully representative. Many of the zoned rims are characterised by relatively high U (600–800, ranging up to 2235 ppm) and low Th with Th/U ≤0.06 with some ≤0.02 suggesting that they are metamorphic. There is also variable enrichment in common Pb. The distribution of $^{206}Pb/^{238}U$ ages shows scatter, but in general there is a grouping of these rim areas around 205–215 Ma and a lesser grouping at about 180–195 Ma (Fig. 4).

4.2. Igneous rocks

Zircons from MEJ-18024 (n = 20) are all igneous with high Th/U ratios between 0.37 and 0.88. Their $^{206}Pb/^{238}U$ ages range from 198 to 212 Ma, with an overall mean of 207 Ma but a rather high MSWD of 2.2. In a probability plot there is a distinct skew to the younger ages, as might be expected if there were slight Pb-loss effects. Ignoring the youngest three ages to allow for this (# 13.1 has a high common P content), the weighted mean age of the remaining 17 grains is 208 ± 2 Ma (MSWD = 1.4), which is taken to date a Late Triassic (Norian) crystallization age (Fig. 5).

The zircons from MEJ-18029 are clearly multi-stage, with grains exhibiting concentric igneous zonation, many of which have overgrowths with exceptionally high U contents (up to 8676 ppm), some of which are metamict (Fig. 6). Crystallization of very high-U zircon in leucogranites is possibly a result of anatexis in an upper crustal environment. The ages (n = 30) spread from ca. 150 Ma to ca. 1450 Ma, but with a clear inverse relationship to U content: all grains with >1000 ppm have ages <211 Ma. The low-U grains have apparent age peaks at ca. 147 Ma, 220–220 Ma, 290, and 485 Ma, as well as scattered single ages at 1000–1450 Ma (Fig. 5), which must represent inheritance from a sedimentary source. The single age of 147 Ma has been ignored as it requires an extremely high common Pb correction compared to the other data, so that the leucogranite must have acquired its inherited components during a melting event younger than 200 Ma. The ages of the high-U group range from 211 Ma down to 164 Ma; six of these ages are consistent, yielding a weighted mean of 180 ± 2 Ma (MSWD = 1.3). This would normally be interpreted as dating crystallization of the granite, but could not explain the fact that seven of the high-U overgrowths give older ages. Alternatively, since Pb-loss would have been facilitated by the radiation-damaged structure of metamict zircon (e.g., Mezger and Krogstad, 2004) it is possible that this resulted from a thermal overprint during emplacement of the nearby Jurassic batholith, and that the original age of the anatexis event that produced the leucogranite was ca. 210 Ma.

MEJ-18031 zircons are very large simple, prismatic and of igneous appearance. Ages (n = 20) are very consistent: ignoring the one apparent outlier at 165 Ma, the weighted average age of 19 grains is 184 ± 1 Ma (MSWD = 1.04), i.e., Pliensbachian (Early Jurassic). This is taken as the age of magmatic crystallization (Fig. 5).

5. Discussion

5.1. Summary of U–Pb SHRIMP results

In the northern block the maximum possible sedimentary age of the protolith to sample MEJ-18025 (ca. 210 Ma) and the crystallization age of the Morro de Mejillones pluton hornblende–biotite

Table 2
Summary of SHRIMP U–Pb zircon results for Mejillones metasedimentary samples.

							Total ratios				Radiogenic ratios							Age (Ma)				
Grain spot	U (ppm)	Th (ppm)	Th/U	^{206}Pb[a] (ppm)	$^{204}Pb/^{206}Pb$	f_{206} %	$^{238}U/^{206}Pb$	±	$^{207}Pb/^{206}Pb$	±	$^{206}Pb/^{238}U$	±	$^{207}Pb/^{235}U$	±	$^{207}Pb/^{206}Pb$	±	ρ	$^{206}Pb/^{238}U$	±	$^{207}Pb/^{206}Pb$	±	% disc
MEJ-18025 banded gneiss, northern block																						
1.1	145	93	0.64	10	0.000295	0.01	11.924	0.161	0.0578	0.0010	0.0839	0.0012						519	7			
2.1	279	291	1.04	21	0.000159	<0.01	11.382	0.136	0.0575	0.0010	0.0880	0.0011						543	6			
3.1	918	415	0.45	43	0.000030	0.03	18.525	0.199	0.0535	0.0005	0.0540	0.0006						339	4			
[a]4.1	78	73	0.93	0	0.019185	22.01	294.9	12.6	0.2204	0.0555	0.0026	0.0003						17	2			
5.1	817	439	0.54	58	0.000077	<0.01	12.156	0.130	0.0573	0.0004	0.0823	0.0009						510	5			
6.1	397	57	0.14	34	0.000061	0.06	9.950	0.117	0.0608	0.0006	0.1004	0.0012						617	7			
7.1	204	98	0.48	6	0.000303	0.34	29.884	0.451	0.0530	0.0013	0.0334	0.0005						211	3			
8.1	274	19	0.07	19	0.000135	0.05	12.088	0.144	0.0580	0.0007	0.0827	0.0010						512	6			
[a]9.1	902	103	0.11	146	0.000065	0.11	5.308	0.057	0.1038	0.0006	0.1882	0.0020	2.670	0.033	0.1029	0.0006	0.881	1112	11	1677	11	34
10.1	491	15	0.03	74	0.000002	<0.01	5.688	0.065	0.0742	0.0027	0.1758	0.0020	1.798	0.068	0.0742	0.0027	0.300	1044	11	1047	73	0
11.1	282	163	0.58	14	–	<0.01	17.620	0.216	0.0533	0.0008	0.0568	0.0007						356	4			
12.1	371	108	0.29	52	0.000051	0.09	6.118	0.090	0.0724	0.0012	0.1633	0.0024	1.614	0.036	0.0717	0.0012	0.662	975	13	976	34	0
13.1	198	73	0.37	15	0.000054	0.15	11.269	0.143	0.0597	0.0009	0.0886	0.0011						547	7			
14.1	453	293	0.65	30	0.000089	<0.01	12.805	0.146	0.0561	0.0006	0.0782	0.0009						485	5			
15.1	253	92	0.36	7	0.000772	0.42	29.044	0.408	0.0538	0.0013	0.0343	0.0005						217	3			
16.1	203	186	0.92	19	–	0.69	9.199	0.117	0.0673	0.0008	0.1080	0.0014						661	8			
17.1	504	200	0.40	39	–	<0.01	11.058	0.125	0.0583	0.0005	0.0905	0.0010						558	6			
18.1	542	844	1.56	47	0.000072	0.10	9.829	0.109	0.0614	0.0005	0.1016	0.0011						624	7			
19.1	215	110	0.51	9	0.000184	0.38	20.805	0.287	0.0554	0.0011	0.0479	0.0007						302	4			
20.1	426	159	0.37	16	0.001951	0.40	22.799	0.312	0.0550	0.0013	0.0437	0.0006						276	4			
21.1	222	127	0.57	6	0.000510	0.14	30.225	0.426	0.0514	0.0012	0.0330	0.0005						210	3			
22.1	193	37	0.19	29	0.000055	0.09	5.687	0.075	0.0726	0.0007	0.1758	0.0024	1.752	0.042	0.0723	0.0011	0.781	1044	13	994	32	−5
23.1	245	131	0.53	60	0.000027	0.04	3.519	0.042	0.1008	0.0022	0.2840	0.0034	3.935	0.100	0.1005	0.0023	0.466	1612	17	1633	42	1
24.1	151	90	0.60	26	0.000109	0.18	5.021	0.066	0.0817	0.0008	0.1988	0.0026	2.198	0.047	0.0802	0.0013	0.618	1169	14	1202	33	3
25.1	238	105	0.44	9	0.006758	1.95	22.439	0.385	0.0674	0.0021	0.0437	0.0008						276	5			
26.1	339	73	0.22	25	0.001181	1.44	11.427	0.141	0.0699	0.0008	0.0862	0.0011						533	6			
[a]27.1	1311	186	0.14	74	0.003810	7.12	15.221	0.164	0.1117	0.0020	0.0610	0.0007						382	4			
28.1	180	68	0.38	8	0.000083	<0.01	18.516	0.283	0.0524	0.0023	0.0541	0.0008						339	5			
29.1	792	154	0.19	185	0.000022	0.04	3.669	0.043	0.1039	0.0006	0.2724	0.0032	3.893	0.050	0.1036	0.0006	0.899	1553	16	1690	10	8
30.1	854	237	0.28	55	0.000256	0.42	13.362	0.243	0.0597	0.0006	0.0745	0.0014						463	8			
Error in Temora reference zircon calibration was 0.62% for the analytical session.																						
FO0928 biotite schist, northern block																						
1.1	308	58	0.19	22	0.000051	0.15	11.947	0.136	0.0589	0.0007	0.0836	0.0010						517	6			
2.1	444	47	0.11	49	–	<0.01	7.753	0.086	0.0697	0.0005	0.1290	0.0014	1.246	0.017	0.0700	0.0006	0.809	782	8	929	17	16
3.1	117	51	0.44	17	0.000221	0.38	5.890	0.073	0.0762	0.0009	0.1691	0.0021	1.704	0.046	0.0731	0.0017	0.469	1007	12	1016	48	1
[a]4.1	42	0	0.00	3	–	6.84	10.722	0.180	0.1139	0.0386	0.0869	0.0047						537	28			
[a]5.1	285	90	0.31	3	–	45.43	79.097	1.192	0.4067	0.0061	0.0069	0.0002						44	1			
[a]6.1	224	93	0.41	14	0.001232	7.16	13.475	0.241	0.1134	0.0278	0.0689	0.0029						430	17			
7.1	777	55	0.07	114	0.000095	0.16	5.847	0.062	0.0727	0.0003	0.1707	0.0018	1.681	0.022	0.0714	0.0005	0.830	1016	10	968	15	−5
8.1	116	93	0.80	7	0.000327	0.35	13.370	0.182	0.0591	0.0013	0.0745	0.0010						463	6			
9.1	382	94	0.25	25	0.000032	0.10	13.220	0.149	0.0572	0.0007	0.0756	0.0009						470	5			
10.1	280	41	0.15	18	0.000020	0.16	13.100	0.152	0.0578	0.0007	0.0762	0.0009						473	5			
11.1	153	27	0.18	29	0.000139	0.23	4.593	0.056	0.0842	0.0009	0.2172	0.0027	2.465	0.057	0.0823	0.0016	0.536	1267	14	1252	38	−1
12.1	233	103	0.44	14	0.000121	0.49	14.352	0.179	0.0595	0.0010	0.0693	0.0009						432	5			
13.1	599	61	0.10	43	0.000103	0.65	11.927	0.128	0.0629	0.0005	0.0833	0.0009						516	5			
14.1	339	203	0.60	16	–	0.27	17.804	0.208	0.0557	0.0008	0.0560	0.0007						351	4			
15.1	61	50	0.82	10	0.000415	0.70	5.317	0.075	0.0903	0.0013	0.1867	0.0027	2.174	0.093	0.0844	0.0034	0.338	1104	15	1302	78	15
16.1	191	56	0.30	35	0.000087	0.14	4.673	0.056	0.0810	0.0007	0.2137	0.0025	2.350	0.038	0.0798	0.0009	0.735	1248	14	1191	22	−5
17.1	549	175	0.32	93	0.000157	0.26	5.090	0.055	0.0803	0.0004	0.1959	0.0021	2.109	0.028	0.0781	0.0006	0.801	1153	11	1149	16	0
18.1	640	25	0.04	46	–	0.31	12.001	0.129	0.0601	0.0005	0.0831	0.0009						514	5			
19.1	65	31	0.47	4	0.000292	0.75	13.234	0.201	0.0624	0.0016	0.0750	0.0012						466	7			
20.1	91	34	0.38	36	0.000038	0.05	2.139	0.026	0.1767	0.0010	0.4673	0.0058	11.356	0.156	0.1762	0.0011	0.898	2472	25	2618	10	6
21.1	226	103	0.46	48	0.000021	0.03	4.013	0.063	0.1042	0.0023	0.2491	0.0039	3.568	0.099	0.1039	0.0024	0.572	1434	20	1694	42	15
22.1	61	25	0.41	9	0.000133	0.23	5.690	0.079	0.0796	0.0012	0.1753	0.0024	1.880	0.050	0.0777	0.0018	0.524	1042	13	1140	45	9
23.1	646	297	0.46	38	0.000096	0.27	14.536	0.155	0.0576	0.0005	0.0686	0.0007						428	4			

(continued on next page)

Table 2 (*continued*)

Grain spot	U (ppm)	Th (ppm)	Th/U	^{206}Pb[a] (ppm)	$^{204}Pb/^{206}Pb$	f_{206} %	Total ratios				Radiogenic ratios						ρ	Age (Ma)				
							$^{238}U/^{206}Pb$	±	$^{207}Pb/^{206}Pb$	±	$^{206}Pb/^{238}U$	±	$^{207}Pb/^{235}U$	±	$^{207}Pb/^{206}Pb$	±		$^{206}Pb/^{238}U$	±	$^{207}Pb/^{206}Pb$	±	% disc
[a]24.1	200	165	0.83	6	0.005953	9.65	28.706	0.384	0.1271	0.0077	0.0315	0.0005						200	3			
25.1	214	22	0.10	14	0.000476	0.34	13.338	0.157	0.0591	0.0009	0.0747	0.0009						465	5			
26.1	238	76	0.32	15	0.000108	0.04	13.320	0.155	0.0567	0.0008	0.0750	0.0009						466	5			
27.1	567	205	0.36	68	–	<0.01	7.166	0.076	0.0703	0.0004	0.1396	0.0015	1.363	0.017	0.0708	0.0005	0.838	843	8	951	14	11
28.1	137	13	0.09	9	0.000818	1.89	13.284	0.175	0.0715	0.0011	0.0739	0.0010						459	6			
29.1	456	247	0.54	28	0.000209	0.35	13.798	0.150	0.0587	0.0006	0.0722	0.0008						450	5			
30.1	217	2	0.01	29	0.000007	0.01	6.446	0.075	0.0742	0.0012	0.1551	0.0018	1.585	0.031	0.0741	0.0012	0.587	930	10	1044	32	11
31.1	528	260	0.49	32	0.000049	0.19	14.226	0.155	0.0572	0.0006	0.0702	0.0008						437	5			
32.1	388	31	0.08	25	0.000001	0.07	13.191	0.150	0.0570	0.0006	0.0758	0.0009						471	5			
33.1	189	112	0.59	13	0.000131	<0.01	12.802	0.154	0.0564	0.0009	0.0782	0.0010						485	6			
[a]34.1	86	16	0.19	12	0.002652	4.55	6.075	0.179	0.0977	0.0105	0.1571	0.0048	1.282	0.284	0.0592	0.0130	0.138	941	27	574	478	−64
35.1	459	183	0.40	21	0.000186	<0.01	18.544	0.205	0.0532	0.0006	0.0539	0.0006						339	4			
36.1	255	162	0.63	16	0.000051	0.02	13.871	0.173	0.0561	0.0009	0.0721	0.0009						449	5			
37.1	138	72	0.53	20	0.000014	0.02	5.875	0.072	0.0743	0.0008	0.1702	0.0021	1.738	0.029	0.0741	0.0008	0.730	1013	11	1043	23	3
[a]38.1	204	124	0.61	5	–	0.32	32.375	0.430	0.0526	0.0014	0.0308	0.0004						195	3			
39.1	768	496	0.65	49	0.000058	0.12	13.346	0.144	0.0573	0.0004	0.0748	0.0008						465	5			
40.1	362	13	0.04	25	0.000007	0.55	12.538	0.142	0.0615	0.0007	0.0793	0.0009						492	5			
41.1	359	66	0.18	24	0.000187	0.04	12.860	0.146	0.0571	0.0007	0.0777	0.0009						483	5			
42.1	434	103	0.24	67	0.000033	0.06	5.571	0.063	0.0796	0.0005	0.1794	0.0020	1.959	0.026	0.0792	0.0006	0.840	1064	11	1177	14	10
43.1	347	121	0.35	62	0.000010	0.02	4.824	0.053	0.0814	0.0005	0.2072	0.0023	2.321	0.030	0.0812	0.0005	0.864	1214	12	1227	13	1
44.1	106	59	0.56	18	0.000068	0.11	5.108	0.066	0.0805	0.0009	0.1955	0.0025	2.144	0.045	0.0795	0.0013	0.612	1151	14	1185	33	3
45.1	128	72	0.56	9	0.000475	0.23	11.913	0.158	0.0596	0.0012	0.0838	0.0011						518	7			
46.1	702	12	0.02	48	0.000001	0.09	12.541	0.135	0.0578	0.0005	0.0797	0.0009						494	5			
47.1	111	68	0.62	23	–	<0.01	4.201	0.055	0.0891	0.0009	0.2382	0.0031	2.946	0.053	0.0897	0.0011	0.729	1377	16	1419	23	3
48.1	397	120	0.30	77	0.000052	0.09	4.457	0.049	0.0874	0.0005	0.2242	0.0024	2.680	0.034	0.0867	0.0006	0.851	1304	13	1354	13	4
[a]49.1	148	164	1.11	3	–	<0.01	38.918	0.600	0.0478	0.0031	0.0257	0.0004						164	3			
50.1	548	92	0.17	37	0.000019	0.18	12.577	0.139	0.0585	0.0006	0.0794	0.0009						492	5			
51.1	75	68	0.91	20	–	<0.01	3.160	0.044	0.1142	0.0011	0.3166	0.0044	4.994	0.085	0.1144	0.0011	0.814	1773	22	1871	18	5
52.1	247	60	0.24	17	0.000097	0.09	12.386	0.152	0.0580	0.0009	0.0807	0.0010						500	6			
53.1	310	12	0.04	25	–	0.58	10.752	0.127	0.0638	0.0008	0.0925	0.0011						570	7			
54.1	178	150	0.84	11	0.000060	0.34	13.923	0.175	0.0586	0.0010	0.0716	0.0009						446	6			
55.1	62	12	0.19	6	0.000243	0.61	8.516	0.131	0.0681	0.0017	0.1167	0.0019						712	11			
56.1	184	84	0.46	33	0.000002	<0.01	4.787	0.057	0.0810	0.0007	0.2089	0.0025	2.331	0.034	0.0809	0.0007	0.805	1223	13	1220	17	0
57.1	506	126	0.25	97	0.000005	0.01	4.462	0.048	0.0969	0.0008	0.2241	0.0024	2.993	0.040	0.0969	0.0008	0.809	1304	13	1565	15	17
58.1	524	160	0.31	95	0.000040	0.07	4.743	0.051	0.0822	0.0007	0.2107	0.0023	2.372	0.034	0.0817	0.0008	0.761	1233	12	1237	18	0
59.1	342	205	0.60	22	0.000250	<0.01	13.510	0.162	0.0562	0.0007	0.0740	0.0009						460	5			
60.1	825	77	0.09	57	0.000005	0.30	12.427	0.131	0.0596	0.0004	0.0802	0.0009						497	5			
Error in Temora reference zircon calibration was 0.94% for the analytical session.																						
MEJ-18030 banded gneiss, central block																						
1.1	278	226	0.82	11	0.000110	0.10	21.430	0.258	0.0530	0.0008	0.0466	0.0006						294	3			
2.1	264	102	0.39	32	0.000029	0.05	7.179	0.082	0.0669	0.0005	0.1392	0.0016	1.275	0.018	0.0664	0.0005	0.818	840	9	820	17	−2
3.1	382	645	1.69	32	0.000057	<0.01	10.191	0.110	0.0592	0.0004	0.0982	0.0011						604	6			
4.1	110	48	0.44	19	–	<0.01	5.068	0.061	0.0767	0.0007	0.1973	0.0024	2.087	0.031	0.0767	0.0007	0.807	1161	13	1114	18	−4
5.1	262	27	0.10	18	0.000081	−0.10	12.783	0.147	0.0560	0.0006	0.0783	0.0009						486	5			
6.1	334	53	0.16	23	–	<0.01	12.319	0.156	0.0593	0.0005	0.0810	0.0010						502	6			
7.1	286	386	1.35	12	0.000179	<0.01	20.979	0.244	0.0522	0.0007	0.0477	0.0006						300	3			
8.1	285	161	0.57	12	0.000139	0.43	20.701	0.241	0.0558	0.0008	0.0481	0.0006						303	3			
9.1	640	543	0.85	108	0.000008	0.01	5.088	0.055	0.0804	0.0004	0.1965	0.0021	2.174	0.025	0.0802	0.0004	0.922	1157	11	1203	9	4
10.1	275	268	0.98	11	–	<0.01	22.310	0.274	0.0516	0.0009	0.0448	0.0006						283	3			
11.1	461	28	0.06	31	0.000020	0.04	12.825	0.143	0.0572	0.0006	0.0779	0.0009						484	5			
12.1	577	59	0.10	38	0.000057	<0.01	12.938	0.142	0.0566	0.0005	0.0773	0.0009						480	5			
13.1	345	198	0.57	17	0.000055	<0.01	17.815	0.211	0.0520	0.0008	0.0562	0.0007						353	4			
14.1	649	48	0.07	43	0.000020	<0.01	13.105	0.143	0.0563	0.0005	0.0763	0.0008						474	5			
[a]15.1	235	144	0.61	2	0.000368	0.38	110.48	1.93	0.0502	0.0022	0.0090	0.0002						58	1			
16.1	45	1	0.01	1	–	2.24	30.328	0.775	0.0681	0.0038	0.0322	0.0008						205	5			
16.2	495	512	1.03	33	–	<0.01	13.062	0.146	0.0561	0.0006	0.0766	0.0009						476	5			
17.1	585	302	0.52	20	0.000101	0.04	24.805	0.284	0.0517	0.0007	0.0403	0.0005						255	3			
18.1	272	38	0.14	49	0.000021	0.04	4.798	0.056	0.0869	0.0006	0.2084	0.0024	2.489	0.034	0.0866	0.0006	0.851	1220	13	1352	14	10

19.1	113	79	0.71	17	–	<0.01	5.696	0.076	0.0730	0.0012	0.1756	0.0023	1.766	0.036	0.0730	0.0012	0.644	1043	13	1013	32	−3
20.1	558	332	0.60	88	0.000038	0.06	5.459	0.058	0.0772	0.0004	0.1831	0.0020	1.936	0.024	0.0767	0.0005	0.868	1084	11	1114	12	3
21.1	462	402	0.87	19	0.000123	<0.01	20.470	0.235	0.0517	0.0007	0.0489	0.0006						308	3			
22.1	1407	1285	0.91	55	0.000096	0.11	21.901	0.231	0.0529	0.0004	0.0456	0.0005						288	3			
23.1	96	26	0.27	5	0.000591	0.04	17.604	0.279	0.0540	0.0015	0.0568	0.0009						356	6			
24.1	434	34	0.08	63	0.000011	0.02	5.929	0.094	0.0716	0.0014	0.1689	0.0027	1.693	0.044	0.0727	0.0014	0.682	1006	15	1005	39	0
25.1	240	72	0.30	12	–	0.59	17.505	0.226	0.0584	0.0010	0.0568	0.0007						356	5			
26.1	153	43	0.28	11	–	1.66	12.179	0.173	0.0708	0.0011	0.0807	0.0012						501	7			
27.1	222	85	0.38	8	0.000260	0.07	24.415	0.327	0.0520	0.0012	0.0409	0.0006						259	3			
28.1	173	127	0.74	6	0.000398	0.36	25.735	0.355	0.0539	0.0013	0.0387	0.0005						245	3			
29.1	43	24	0.57	19	–	<0.01	1.936	0.033	0.1846	0.0015	0.5166	0.0088	13.147	0.248	0.1846	0.0015	0.907	2685	38	2694	13	0
30.1	454	187	0.41	27	0.000027	0.19	14.498	0.162	0.0570	0.0006	0.0688	0.0008						429	5			
31.1	183	87	0.47	10	–	0.33	15.257	0.198	0.0575	0.0010	0.0653	0.0009						408	5			
32.1	395	319	0.81	34	0.000073	0.12	10.002	0.116	0.0612	0.0006	0.0999	0.0012						614	7			
33.1	285	108	0.38	12	0.000107	0.25	20.016	0.247	0.0546	0.0009	0.0498	0.0006						314	4			
33.2	199	110	0.55	9	0.000236	0.09	19.460	0.255	0.0535	0.0010	0.0513	0.0007						323	4			
34.1	419	57	0.14	27	0.000014	0.08	13.300	0.150	0.0570	0.0006	0.0751	0.0009						467	5			
35.1	436	256	0.59	30	–	0.09	12.523	0.140	0.0578	0.0009	0.0798	0.0009						495	5			
36.1	174	111	0.64	41	0.000931	1.50	3.655	0.045	0.1186	0.0014	0.2695	0.0033	3.934	0.090	0.1059	0.0020	0.541	1538	17	1729	35	11
37.1	516	27	0.05	25	–	0.22	17.780	0.203	0.0554	0.0008	0.0561	0.0006						352	4			
37.2	242	70	0.29	18	0.000127	0.04	11.514	0.139	0.0585	0.0008	0.0868	0.0011						537	6			
38.1	560	69	0.12	45	–	<0.01	10.646	0.116	0.0588	0.0005	0.0940	0.0010						579	6			
39.1	242	148	0.61	11	0.000174	0.36	19.413	0.239	0.0558	0.0009	0.0513	0.0006						323	4			
40.1	1043	1101	1.06	41	0.000081	0.04	21.606	0.234	0.0524	0.0004	0.0463	0.0005						292	3			
Error in Temora reference zircon calibration was 0.44% for the analytical session.																						
F00930 Micaschist, central block																						
1.1	335	49	0.15	8	–	0.38	36.824	0.512	0.0526	0.0023	0.0271	0.0004						172	2			
[a]2.1	271	109	0.40	38	0.000251	0.43	6.156	0.069	0.0843	0.0006	0.1618	0.0018	1.802	0.032	0.0808	0.0011	0.632	967	10	1216	27	21
3.1	1235	244	0.20	157	0.000009	0.02	6.755	0.070	0.0736	0.0003	0.1480	0.0015	1.499	0.017	0.0734	0.0003	0.913	890	9	1026	9	13
4.1	209	60	0.29	32	0.000089	0.15	5.663	0.068	0.0821	0.0008	0.1763	0.0021	1.966	0.039	0.0809	0.0013	0.609	1047	12	1218	31	14
5.1	223	173	0.78	14	0.000428	0.42	13.575	0.167	0.0595	0.0010	0.0734	0.0009						456	6			
6.1	191	73	0.38	24	0.000234	0.40	6.774	0.111	0.0748	0.0016	0.1470	0.0025	1.448	0.078	0.0714	0.0037	0.310	884	14	969	105	9
[a]7.1	229	182	0.79	6	0.002029	4.29	32.546	0.714	0.0840	0.0037	0.0294	0.0007						187	4			
8.1	319	174	0.55	35	0.000093	0.16	7.732	0.095	0.0728	0.0011	0.1291	0.0016	1.273	0.026	0.0715	0.0012	0.595	783	9	972	34	19
9.1	261	1	0.00	24	0.000135	0.11	9.460	0.120	0.0621	0.0005	0.1056	0.0014						647	8			
10.1	158	65	0.41	7	0.000642	0.99	20.389	0.252	0.0604	0.0011	0.0486	0.0006						306	4			
11.1	225	38	0.17	15	0.000130	<0.01	12.800	0.147	0.0568	0.0007	0.0781	0.0009						485	5			
12.1	886	447	0.50	58	–	<0.01	13.106	0.137	0.0560	0.0004	0.0764	0.0008						474	5			
13.1	579	156	0.27	39	–	0.34	12.677	0.147	0.0596	0.0005	0.0786	0.0009						488	6			
14.1	39	11	0.28	6	0.000193	0.33	6.130	0.101	0.0711	0.0015	0.1629	0.0028	1.577	0.069	0.0702	0.0024	0.656	973	16	933	71	−4
15.1	226	117	0.52	7	0.000040	<0.01	29.030	0.358	0.0490	0.0011	0.0345	0.0004						219	3			
16.1	214	96	0.45	14	0.000195	0.31	13.040	0.160	0.0591	0.0008	0.0765	0.0010						475	6			
17.1	111	85	0.76	8	–	<0.01	12.673	0.165	0.0554	0.0011	0.0791	0.0010						490	6			
18.1	318	297	0.93	18	–	<0.01	15.177	0.170	0.0536	0.0006	0.0660	0.0007						412	5			
19.1	618	216	0.35	22	0.000157	0.16	24.525	0.266	0.0526	0.0006	0.0407	0.0004						257	3			
20.1	166	134	0.81	50	0.000017	0.03	2.848	0.032	0.1204	0.0006	0.3510	0.0040	5.815	0.073	0.1202	0.0007	0.902	1939	19	1959	10	1
21.1	232	274	1.18	39	–	<0.01	5.065	0.058	0.0763	0.0006	0.1975	0.0023	2.086	0.029	0.0766	0.0006	0.809	1162	12	1110	17	−5
22.1	358	148	0.41	58	0.000094	0.16	5.348	0.059	0.0805	0.0005	0.1867	0.0021	2.039	0.031	0.0792	0.0008	0.725	1103	11	1177	21	6
23.1	140	77	0.55	9	–	<0.01	13.708	0.171	0.0560	0.0010	0.0730	0.0009						454	6			
24.1	236	184	0.78	17	0.000093	0.06	11.993	0.137	0.0581	0.0008	0.0833	0.0010						516	6			
25.1	591	29	0.05	40	0.000024	0.02	12.721	0.135	0.0571	0.0005	0.0786	0.0009						488	5			
26.1	289	75	0.26	33	0.000094	0.16	7.485	0.084	0.0692	0.0006	0.1334	0.0015	1.247	0.022	0.0678	0.0009	0.653	807	9	863	27	6
27.1	411	296	0.72	31	0.000058	0.08	11.299	0.130	0.0591	0.0006	0.0884	0.0010						546	6			
28.1	715	316	0.44	50	0.000245	0.28	12.270	0.132	0.0596	0.0005	0.0813	0.0009						504	5			
29.1	55	0	0.00	3	0.000745	0.36	15.365	0.286	0.0578	0.0080	0.0648	0.0014						405	8			
30.1	165	64	0.39	25	0.000074	0.13	5.640	0.070	0.0814	0.0093	0.1771	0.0022	1.961	0.229	0.0803	0.0093	0.106	1051	12	1205	229	13
[a]31.1	152	181	1.19	3	0.000572	1.06	43.448	0.633	0.4171	0.1079	0.0228	0.0004	1.295	0.343	0.4125	0.1091	0.063	145	2			
32.1	572	38	0.07	44	–	0.21	11.151	0.120	0.0603	0.0036	0.0895	0.0011						553	6			
33.1	825	33	0.04	86	0.000060	0.10	8.257	0.088	0.0688	0.0005	0.1210	0.0013	1.133	0.016	0.0679	0.0006	0.776	736	7	867	18	15
34.1	295	82	0.28	52	0.000081	0.14	4.830	0.055	0.0839	0.0005	0.2068	0.0024	2.360	0.034	0.0828	0.0007	0.785	1211	13	1264	18	4
35.1	144	125	0.87	12	0.000065	0.02	10.263	0.133	0.0601	0.0010	0.0974	0.0013						599	8			
36.1	268	293	1.09	37	0.000001	<0.01	6.234	0.071	0.0707	0.0006	0.1604	0.0018	1.564	0.022	0.0707	0.0006	0.796	959	10	949	18	−1

(continued on next page)

Table 2 (*continued*)

Grain spot	U (ppm)	Th (ppm)	Th/U	^{206}Pb[a] (ppm)	$^{204}Pb/^{206}Pb$	f_{206} %	Total ratios				Radiogenic ratios						ρ	Age (Ma)				
							$^{238}U/^{206}Pb$	±	$^{207}Pb/^{206}Pb$	±	$^{206}Pb/^{238}U$	±	$^{207}Pb/^{235}U$	±	$^{207}Pb/^{206}Pb$	±		$^{206}Pb/^{238}U$	±	$^{207}Pb/^{206}Pb$	±	% disc
37.1	207	86	0.42	32	–	<0.01	5.640	0.066	0.0740	0.0007	0.1773	0.0021	1.813	0.028	0.0742	0.0007	0.777	1052	11	1046	19	−1
38.1	658	208	0.32	76	–	<0.01	7.415	0.080	0.0660	0.0004	0.1349	0.0015	1.232	0.016	0.0662	0.0005	0.839	816	8	814	15	0
39.1	923	279	0.30	117	0.000037	0.06	6.790	0.072	0.0676	0.0003	0.1472	0.0016	1.361	0.017	0.0671	0.0004	0.876	885	9	840	12	−5
40.1	307	140	0.46	20	0.000164	0.25	13.222	0.151	0.0585	0.0007	0.0754	0.0009						469	5			
Error in Temora reference zircon calibration was 0.94% & 0.67% for the analytical sessions.																						
FO1139 Mica schist, central block																						
1.1	117	90	0.77	9	0.000420	0.37	11.658	0.172	0.0610	0.0012	0.0855	0.0013						529	8			
1.2	1239	98	0.08	33	0.003872	6.37	31.833	0.389	0.1007	0.0032	0.0294	0.0004						187	2			
2.1	328	5	0.02	10	0.000972	2.41	28.599	0.367	0.0697	0.0012	0.0341	0.0004						216	3			
2.2	1367	482	0.35	54	0.000132	0.17	21.881	0.252	0.0534	0.0005	0.0456	0.0005						288	3			
2.3	771	968	1.26	30	0.000076	0.13	21.968	0.267	0.0530	0.0006	0.0455	0.0006						287	3			
3.1	928	11	0.01	26	0.000371	0.35	30.448	0.379	0.0531	0.0008	0.0327	0.0004						208	3			
3.2	215	215	1.00	10	0.000405	0.29	19.365	0.253	0.0552	0.0010	0.0515	0.0007						324	4			
4.1	848	50	0.06	22	0.001784	3.90	33.888	0.425	0.0808	0.0011	0.0284	0.0004						180	2			
4.2	536	32	0.06	34	0.000636	1.18	13.744	0.164	0.0654	0.0008	0.0719	0.0009						448	5			
5.1	1176	14	0.01	31	0.000237	0.63	33.131	0.391	0.0549	0.0008	0.0300	0.0004						191	2			
5.2	62	46	0.74	4	0.000382	1.43	12.824	0.206	0.0682	0.0019	0.0769	0.0013						477	8			
6.1	934	27	0.03	29	0.000317	0.87	27.945	0.328	0.0576	0.0006	0.0355	0.0004						225	3			
6.2	257	78	0.30	44	0.000067	0.20	5.013	0.061	0.0806	0.0006	0.1991	0.0025						1170	14			
7.1	643	30	0.05	17	0.002218	4.30	33.180	0.413	0.0841	0.0035	0.0288	0.0004						183	2			
7.2	281	185	0.66	12	0.000440	0.44	20.727	0.265	0.0559	0.0009	0.0480	0.0006						302	4			
8.1	896	7	0.01	26	0.000234	0.39	29.486	0.354	0.0536	0.0006	0.0338	0.0004						214	3			
8.2	2234	26	0.01	62	0.000107	0.20	30.828	0.352	0.0518	0.0004	0.0324	0.0004						205	2			
8.3	452	282	0.63	27	0.000066	0.08	14.391	0.171	0.0562	0.0006	0.0694	0.0008						433	5			
9.1	1228	60	0.05	37	0.001382	2.77	28.830	0.379	0.0726	0.0013	0.0337	0.0004						214	3			
10.1	498	251	0.50	37	0.000060	0.06	11.653	0.138	0.0585	0.0005	0.0858	0.0010						530	6			
11.1	887	20	0.02	24	0.000085	0.48	32.205	0.382	0.0539	0.0008	0.0309	0.0004						196	2			
12.1	1828	20	0.01	52	0.000389	0.65	30.192	0.356	0.0555	0.0005	0.0329	0.0004						209	2			
13.1	38	1	0.03	1	0.005858	4.51	28.623	0.690	0.0864	0.0043	0.0334	0.0008						212	5			
14.1	66	0	0.00	2	0.001771	2.33	25.716	0.518	0.0697	0.0031	0.0380	0.0008						240	5			
15.1	607	188	0.31	23	0.002228	3.87	22.584	0.280	0.0827	0.0023	0.0426	0.0005						269	3			
Error in Temora reference zircon calibration was 0.33% for the analytical session.																						

Uncertainties given at the1σ level.
f_{206}% denotes the percentage of ^{206}Pb that is common Pb.
For areas older than ~800 Ma correction for common Pb was made using the measured $^{204}Pb/^{206}Pb$ ratio.
For areas younger than ~800 Ma correction for common Pb was made using the measured $^{238}U/^{206}Pb$ and $^{207}Pb/^{206}Pb$ ratios following Tera and Wasserburg (1972) as outlined in Williams (1998).
For % disc, 0% denotes a concordant analysis.
[a] Indicates data not considered reliable (e.g., high-common Pb, not-reliable ages, discordance > 10%).

tonalite (208 ± 2 Ma) are coincident within analytical error. Since the intrusive contacts are discordant to both foliation and folding in the gneiss, and the tonalite itself does not show deformation, it is suggested that the sediment was deposited, buried, deformed and metamorphosed very shortly before magmatism at ca. 210 Ma, i.e., Late Triassic (Norian). In the central block, field evidence and the crystallization age of the garnet-bearing anatectic leucogranite (ca. 210 Ma) suggest that its intrusion was late but essentially coeval with the development of foliation in the host rocks. Metamorphic zircon overgrowth with an age of 205 ± 5 Ma in the gneiss MEJ-18030 reinforces the interpretation drawn from the northern block, suggesting that the first metamorphic event recorded here also took place at ca. 210 Ma. The same conclusion is reached from sample FO1139, which shows metamorphic rim ages between 205 and 215 Ma (Fig. 4).

The maximum sedimentation age of the central block gneiss (MEJ-18030) can be constrained between ca. 205 and 255 Ma, but inherited zircons of 210–220 Ma in the leucogranite suggest that maximum sedimentary ages in this block could also be as young as 210 Ma, similar to those in the northern block. Samples FO0928 and FO09230 contain a few zircons with Jurassic ages. However these rocks show foliations and folds similar to those of the other metasedimentary rocks dealt with here; in consequence those ages are considered to be meaningless.

From the above it becomes clear that metasedimentary rocks that crop out in the northern and central blocks of the Mejillones peninsula are as young as Late Triassic and not Early Paleozoic as suggested by previous geochronological work.

5.2. Comparison with published ages

The 530 Ma Rb–Sr reference isochron of Diaz et al. (1985) for the andalusite-zone schist at Punta Angamos in the northern sector (23°10′S; 70°34′W), based on only 3 out of 6 whole-rock samples, clearly cannot be regarded as significant, nor can other indications of 320 and 255 Ma, due to the low number of analyses and the absence of true isochrons. However, their Rb–Sr WR data for schists from the southern area were shown to fall on a reasonable errorchron given as 200 ± 10 Ma — our recalculation using Isoplot/Ex and with assumed analytical uncertainties results in an isochron (MSWD of 1.2 for 6 out of 8 analyses) with an age of 206 ± 7 Ma, and an initial $^{87}Sr/^{86}Sr$ ratio of 0.7037 ± 0.0002. This is consistent with our conclusions for Late Triassic metamorphism in the northern and central blocks.

With regard to the Sm–Nd WR age of 521 ± 55 Ma for orthoamphibolite from the central outcrop obtained by Damm et al. (1990), we note that the large uncertainty on this age is highly dependant on the assumed analytical precision — a less optimistic estimate would result in a much higher age uncertainty. Support for Paleozoic crystallization was apparently given by these authors' U–Pb zircon discordia age for the Morro Mejillones pluton tonalite of 561 +12/−14 Ma (upper intercept); the 175 ± 10 Ma lower intercept was interpreted as a cooling age. However the published data do not justify construction of a discordia line within assumed uncertainties — our recalculation of these intercepts gives rather meaningless ages of 717 ± 330 and 182 ± 34 Ma with MSWD = 37. We believe that the lower intercept was interpreted more correctly as reflecting the crystallization age by Cortés et al. (2007).

Lucassen et al. (2000) obtained an age of 525 ± 10 Ma from a Sm–Nd mineral isochron from a Morro Jorgino garnet amphibolite. However, in this case the whole-rock analysis does not plot anywhere near the isochron, and the uncertainty reported corresponds to an unusually high estimated precision in the measured Nd isotope ratios (ca. ±0.0005%). Our samples MEJ-18029 and 18030 were collected essentially at the same location and fail to show any evidence for a Cambrian metamorphic age.

5.3. Processes at the Late Triassic pre-Andean margin

SHRIMP evidence from the northern block further suggests that sedimentary protoliths were buried, deformed (foliations and folding) and metamorphosed very rapidly, probably within a very few million years, at ca. 210 Ma. Moreover, the metasedimentary wedge was uplifted and intruded by late arc-related tonalite (Morro Mejillones) within a short time of the peak of metamorphism. The intrusion produced a contact metamorphic aureole (visible in the northern block only) with development of post-S_2 andalusite. The same early tectonometamorphic process also affected the rocks of the central block where a regional Barrovian-type metamorphic zoning (Grt–Ky–Sill) is best displayed (Baeza, 1984). Annealing textures common in this block probably arose from a low-pressure thermal overprint resulting either from a hidden intrusion equivalent to the Morro de Mejillones pluton or from a regional heating event during the emplacement of the Jurassic Bólfin–Punta Tetas arc.

Evidence for igneous activity along the Andean margin at ca. 210 Ma is also provided by the scarce detrital igneous zircons of this age in gneiss MEJ-18025. At least part of the sedimentary pile was sourced from these igneous rocks and the sediments were quickly buried, deformed, metamorphosed and uplifted before the intrusion of the Morro de Mejillones pluton took place at 208 ± 2 Ma. Rapid exhumation is suggested by the formation of andalusite in the contact aureole. The location of this basin in the continental margin remains unknown but it could well be a fore-arc basin or more probably an accretionary frontal wedge where similar fast processes of arc magmatism, erosion, sedimentation, burial, intermediate P/T metamorphism and uplift have been recorded elsewhere (e.g., Matzel and Bowring, 2004; Ducea et al., 2009; Casquet et al., 2012).

The period between the Late Permian and the Late Triassic (Carnian), after the Gondwanide San Rafael orogeny, was essentially extensional along the pre-Andean continental margin, with abundant anorogenic silicic magmatism (part of the Choyoi group) and development of grabens oblique to the margin extending into Argentina. Apparently no subduction took place during this period (Charrier et al., 2007 and references therein).

The arguments produced here for burial of sedimentary rocks, the development of foliation and folding, Barrovian-type metamorphism and arc-magmatism in the Mejillones Peninsula suggest contractional deformation. We infer that this is evidence for renewed subduction along the continental margin in the Late Triassic.

5.4. Source of detrital zircons

Detrital zircons older than Triassic in the metasedimentary rocks from Mejillones Peninsula record many igneous events between 255 and 2700 Ma. The main peaks are Permian, Carboniferous, Ordovician and Cambrian, with sparse Proterozoic ages, many of them of Grenvillian age, i.e., between 0.9 and 1.3 Ga. Events corresponding to these ages are recognized in South America away from the Pacific margin (e.g., in the Sierras Pampeanas and the Cordillera Frontal of Argentina) and in the Andean basement. Thus detrital zircons of the metasedimentary rocks analysed here were either sourced from a foreland extending hundred of kilometres inland, or they were derived through cannibalization of older sedimentary rocks forming the basement of the ca. 210 Ma magmatic arc. The latter possibility is strengthened by evidence from Devonian to Permian turbidite sandstones accreted to the western margin of Gondwana in northern Chile in the late Paleozoic (Bahlburg et al., 2009). Detrital zircon age patterns from these rocks reflect all the orogenic cycles in western Gondwana between 2.0 and 0.25 Ga, as found in the Mejillones samples. Remarkably, a scarcity of Devonian zircons noted by Bahlburg et al. (2009) in the Paleozoic turbidites is also shown by the Mejillones rocks. This absence coincides well with the Devonian hiatus in magmatic activity in northern Chile indicated by Bahlburg and Hervé (1997) and interpreted as indicative of passive margin conditions at that time.

Table 3
Summary of SHRIMP U–Pb zircon results for Mejillones igneous samples.

							Total ratios				Radiogenic ratios							Age (Ma)				
Grain spot	U (ppm)	Th (ppm)	Th/U	^{206}Pb[a] (ppm)	$^{204}Pb/^{206}Pb$	f_{206} %	$^{238}U/^{206}Pb$	±	$^{207}Pb/^{206}Pb$	±	$^{206}Pb/^{238}U$	±	$^{207}Pb/^{235}U$	±	$^{207}Pb/^{206}Pb$	±	ρ	$^{206}Pb/^{238}U$	±	$^{207}Pb/^{206}Pb$	±	% disc
MEJ-18024 Morro Mejillones tonalite																						
1.1	128	61	0.48	3.5	0.001274	0.20	31.80	0.52	0.0517	0.0017	0.0314	0.0005						199.2	3.3			
2.1	133	57	0.43	3.7	0.000210	0.34	30.91	0.49	0.0530	0.0017	0.0322	0.0005						204.6	3.3			
3.1	202	106	0.52	5.6	0.000342	0.60	30.88	0.44	0.0550	0.0014	0.0322	0.0005						204.3	2.9			
4.1	120	45	0.38	3.3	0.001109	<0.01	31.33	0.51	0.0495	0.0022	0.0319	0.0005						202.7	3.3			
5.1	128	72	0.56	3.5	0.001299	0.01	31.71	0.51	0.0502	0.0017	0.0315	0.0005						200.1	3.2			
6.1	384	334	0.87	11.0	0.000005	0.10	30.05	0.38	0.0512	0.0010	0.0332	0.0004						210.8	2.6			
7.1	226	144	0.64	6.4	0.000037	0.40	30.16	0.37	0.0535	0.0012	0.0330	0.0004						209.5	2.6			
8.1	260	135	0.52	7.4	0.000089	0.28	30.02	0.36	0.0526	0.0010	0.0332	0.0004						210.7	2.5			
9.1	137	51	0.37	3.9	0.000486	0.19	30.19	0.43	0.0519	0.0013	0.0331	0.0005						209.6	3.0			
10.1	180	129	0.72	4.9	0.000407	0.11	31.31	0.40	0.0510	0.0011	0.0319	0.0004						202.4	2.6			
11.1	147	78	0.53	4.1	0.000207	0.23	30.80	0.41	0.0521	0.0013	0.0324	0.0004						205.5	2.7			
12.1	208	131	0.63	5.9	–	0.06	30.01	0.38	0.0509	0.0011	0.0333	0.0004						211.2	2.6			
[a] 13.1	178	87	0.49	5.1	0.003249	7.01	29.74	0.47	0.1060	0.0026	0.0313	0.0005						198.5	3.2			
14.1	144	76	0.52	4.1	0.000567	0.36	30.55	0.43	0.0531	0.0014	0.0326	0.0005						206.9	2.9			
15.1	142	58	0.41	4.0	0.000012	<0.01	30.26	0.43	0.0498	0.0014	0.0331	0.0005						209.7	3.0			
16.1	104	38	0.37	3.0	0.000912	0.32	30.16	0.46	0.0529	0.0015	0.0331	0.0005						209.6	3.2			
17.1	269	238	0.88	7.8	0.000270	0.24	29.73	0.37	0.0523	0.0009	0.0336	0.0004						212.8	2.6			
18.1	172	72	0.42	4.8	0.001058	0.53	30.57	0.41	0.0545	0.0012	0.0325	0.0004						206.4	2.8			
19.1	205	107	0.52	5.8	0.000468	0.20	30.32	0.40	0.0519	0.0011	0.0329	0.0004						208.8	2.7			
20.1	203	98	0.48	5.6	0.000165	0.24	31.19	0.41	0.0521	0.0018	0.0320	0.0004						202.9	2.7			
Error in Temora reference zircon calibration was 0.62% for the analytical session.																						
MEJ-18029 Morro Jorgino garnet leucogranite																						
1.1	138	48	0.34	24	0.000122	0.20	4.873	0.060	0.0812	0.0007	0.2048	0.0025	2.243	0.040	0.0794	0.0010	0.688	1201	13	1183	26	−2
2.1	223	153	0.69	12	0.000115	<0.01	15.916	0.192	0.0544	0.0008	0.0628	0.0008						392.9	4.7			
3.1	112	24	0.22	16	0.000083	0.14	6.113	0.080	0.0752	0.0008	0.1634	0.0021	1.668	0.038	0.0741	0.0014	0.576	975	12	1043	37	6
4.1	351	87	0.25	74	0.000014	0.02	4.103	0.046	0.0911	0.0005	0.2437	0.0027	3.053	0.038	0.0909	0.0005	0.904	1406	14	1444	10	3
5.1	167	121	0.73	7	0.000826	0.59	21.231	0.295	0.0570	0.0012	0.0468	0.0007						295.0	4.1			
6.1	684	657	0.96	45	0.000048	0.16	13.076	0.143	0.0579	0.0005	0.0764	0.0008						474.3	5.1			
7.1	511	103	0.20	16	0.001571	3.17	28.331	0.327	0.0758	0.0017	0.0342	0.0004						216.6	2.5			
8.1	773	148	0.19	22	0.001880	3.52	30.578	0.360	0.0782	0.0013	0.0316	0.0004						200.3	2.4			
9.1	417	186	0.45	17	0.000065	0.16	21.614	0.253	0.0534	0.0007	0.0462	0.0005						291.1	3.4			
10.1	279	136	0.49	10	0.000018	0.02	24.510	0.314	0.0515	0.0010	0.0408	0.0005						257.7	3.3			
11.1	156	59	0.38	5	0.000261	0.39	28.404	0.424	0.0537	0.0014	0.0351	0.0005						222.2	3.3			
12.1	2948	32	0.01	71	0.000026	0.05	35.858	0.371	0.0500	0.0003	0.0279	0.0003						177.2	1.8			
13.1	340	216	0.63	23	0.000081	0.04	12.609	0.147	0.0574	0.0007	0.0793	0.0009						491.8	5.6			
14.1	3676	38	0.01	94	0.001109	1.93	33.509	0.348	0.0652	0.0007	0.0293	0.0003						185.9	1.9			
15.1	2953	326	0.11	76	0.000080	<0.01	33.392	0.346	0.0498	0.0003	0.0299	0.0003						190.2	2.0			

16.1	375	499	1.33	13	0.000340	0.06	24.876	0.299	0.0518	0.0008	0.0402	0.0005	253.9	3.0
17.1	5864	480	0.08	159	0.000146	0.13	31.773	0.327	0.0512	0.0004	0.0314	0.0003	199.5	2.0
18.1	1633	329	0.20	38	0.000510	0.97	36.512	0.388	0.0573	0.0005	0.0271	0.0003	172.5	1.8
19.1	8676	239	0.03	245	0.001102	1.92	30.480	0.310	0.0655	0.0007	0.0322	0.0003	204.2	2.1
20.1	2943	756	0.26	71	0.000091	0.09	35.363	0.366	0.0504	0.0003	0.0283	0.0003	179.6	1.8
21.1	3103	430	0.14	76	0.000519	0.96	35.016	0.363	0.0573	0.0004	0.0283	0.0003	179.8	1.8
22.1	3338	74	0.02	88	0.000611	0.51	32.427	0.349	0.0541	0.0006	0.0307	0.0003	194.8	2.1
23.1	4409	87	0.02	127	0.000614	0.68	29.851	0.317	0.0558	0.0004	0.0333	0.0004	211.0	2.2
24.1	3360	466	0.14	83	0.000172	0.25	34.785	0.360	0.0517	0.0003	0.0287	0.0003	182.3	1.9
25.1	2667	57	0.02	60	0.001033	1.93	37.958	0.396	0.0648	0.0008	0.0258	0.0003	164.4	1.7
26.1	1534	318	0.21	35	0.000236	0.33	37.642	0.402	0.0521	0.0005	0.0265	0.0003	168.5	1.8
27.1	8596	1130	0.13	230	0.000983	1.74	32.113	0.325	0.0639	0.0014	0.0306	0.0003	194.3	2.0
28.1	1170	74	0.06	29	0.000093	0.04	34.861	0.377	0.0500	0.0005	0.0287	0.0003	182.2	2.0
29.1	697	209	0.30	33	0.032305	58.03	18.116	0.284	0.5120	0.0289	0.0232	0.0021	147.6	13.4
30.1	1473	42	0.03	38	0.004136	7.96	32.989	0.353	0.1131	0.0035	0.0279	0.0003	177.4	2.1
Error in Temora reference zircon calibration was 0.62% for the analytical session.														
MEJ–18031 Cerro Moreno quartz diorite														
1.1	310	351	1.13	7.6	0.000157	0.19	35.13	0.43	0.0512	0.0009	0.0284	0.0004	180.6	2.2
2.1	232	179	0.77	5.9	–	<0.01	33.99	0.44	0.0494	0.0010	0.0294	0.0004	187.0	2.4
3.1	197	123	0.63	5.0	0.000369	<0.01	34.04	0.43	0.0494	0.0010	0.0294	0.0004	186.8	2.4
4.1	456	529	1.16	11.4	0.000078	0.14	34.24	0.39	0.0509	0.0007	0.0292	0.0003	185.3	2.1
5.1	570	286	0.50	14.0	–	0.04	34.99	0.39	0.0500	0.0006	0.0286	0.0003	181.6	2.0
6.1	358	368	1.03	8.9	0.000022	0.03	34.49	0.40	0.0500	0.0008	0.0290	0.0003	184.2	2.1
7.1	683	712	1.04	17.2	0.000066	0.07	34.12	0.37	0.0504	0.0006	0.0293	0.0003	186.1	2.0
8.1	248	181	0.73	5.5	0.000094	<0.01	38.51	0.50	0.0488	0.0010	0.0260	0.0003	165.4	2.1
9.1	578	691	1.20	14.3	0.000061	<0.01	34.64	0.38	0.0497	0.0006	0.0289	0.0003	183.5	2.0
10.1	443	484	1.09	11.0	0.000066	0.01	34.55	0.39	0.0499	0.0007	0.0289	0.0003	183.9	2.1
11.1	254	211	0.83	6.4	0.000096	0.01	34.00	0.44	0.0499	0.0009	0.0294	0.0004	186.8	2.4
12.1	381	202	0.53	9.4	0.000033	0.05	34.95	0.54	0.0501	0.0008	0.0286	0.0004	181.8	2.8
13.1	257	299	1.16	6.3	0.000096	0.05	34.81	0.43	0.0501	0.0009	0.0287	0.0004	182.5	2.2
14.1	690	898	1.30	17.1	0.000068	<0.01	34.70	0.38	0.0494	0.0006	0.0288	0.0003	183.2	2.0
15.1	715	446	0.62	17.8	0.000049	0.15	34.48	0.37	0.0509	0.0006	0.0290	0.0003	184.0	2.0
16.1	248	230	0.93	6.2	–	<0.01	34.58	0.42	0.0496	0.0012	0.0289	0.0004	183.8	2.2
17.1	540	582	1.08	13.2	0.000076	0.03	35.15	0.40	0.0500	0.0006	0.0284	0.0003	180.8	2.0
18.1	382	429	1.12	9.7	0.000094	<0.01	33.78	0.39	0.0498	0.0008	0.0296	0.0003	188.1	2.2
19.1	388	508	1.31	9.8	0.000109	0.04	33.98	0.39	0.0501	0.0007	0.0294	0.0003	186.9	2.1
20.1	456	543	1.19	11.4	–	0.04	34.51	0.39	0.0501	0.0007	0.0290	0.0003	184.1	2.1
Error in Temora reference zircon calibration was 0.44% for the analytical session.														

Uncertainties given at the1σ level.
f_{206}% denotes the percentage of ^{206}Pb that is common Pb.
For areas older than ~800 Ma correction for common Pb was made using the measured $^{204}Pb/^{206}Pb$ ratio.
For areas younger than ~800 Ma correction for common Pb was made using the measured $^{238}U/^{206}Pb$ and $^{207}Pb/^{206}Pb$ ratios following Tera and Wasserburg (1972) as outlined in Williams (1998).
[a] Indicates data not considered reliable (high-common Pb).

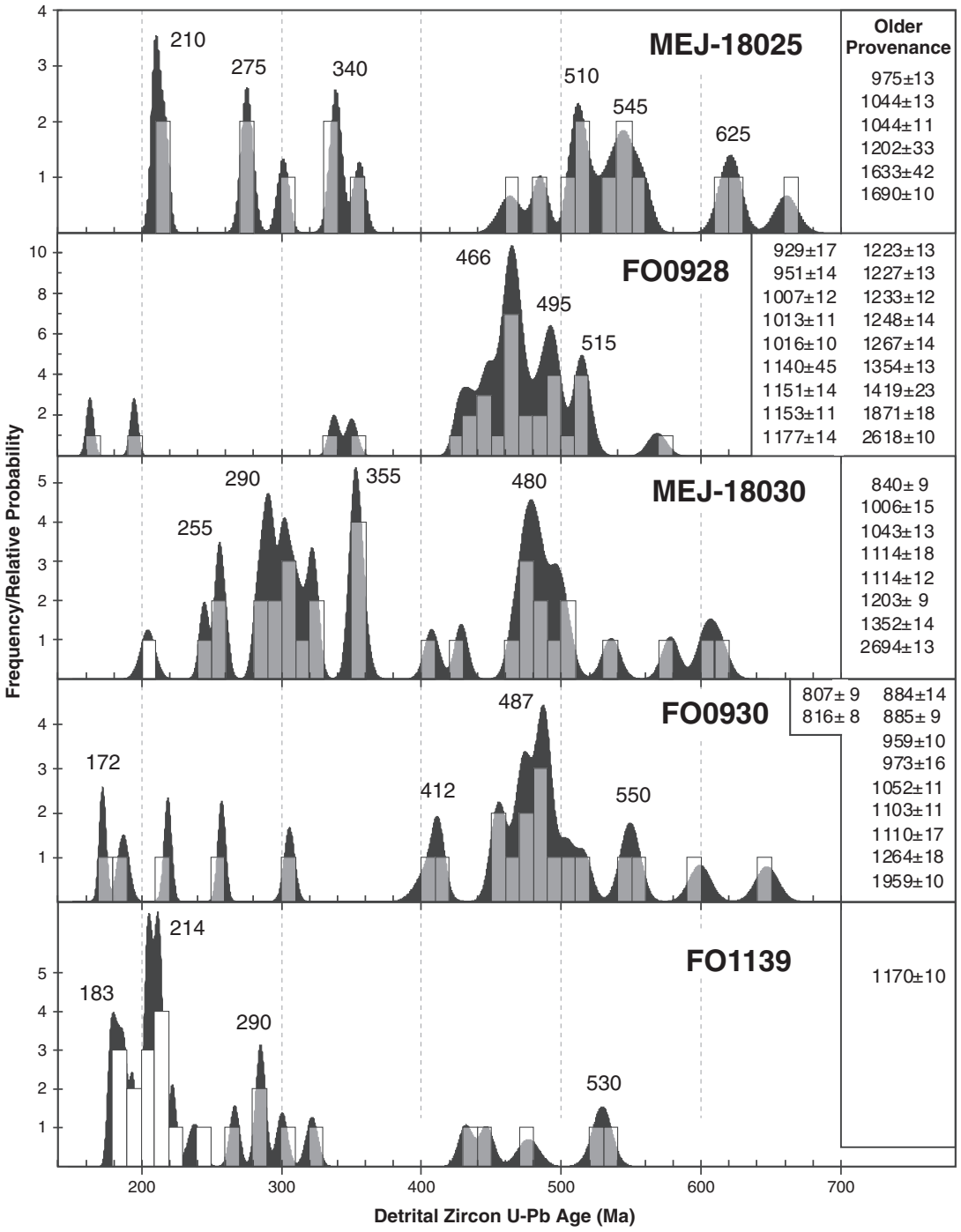

Fig. 4. Partial detrital zircon U–Pb age distribution patterns for Mejillones Peninsula metasedimentary rocks (up to 700 Ma, based on $^{206}Pb/^{238}U$ ages — older age components that are <10% discordant are listed on the right). A few apparent ages younger than mid-Jurassic were eliminated. The approximate ages of the most significant peaks are indicated. Late Triassic to Early Jurassic metamorphic rim ages are distinguished by solid white boxes in the histogram.

Permian zircons were probably sourced from the Choyoi province of mainly silicic volcanic rocks that is widespread in the Frontal Cordillera of Argentina. Llambias (1999) suggested that these rocks were erupted between ca. 260 and 247 Ma, but more recent U–Pb zircon dating of southern parts of the complex shows a more precise age range of ca. 281 to 252 Ma (Rocha-Campos et al., 2011).

5.5. The Jurassic magmatic arc

A crystallization age of 184 ± 1 Ma was recorded for a diorite sample from the Bólfin–Punta Tetas igneous complex in the southern block, reasonably consistent with U–Pb zircon ages of 194 ± 6 and 191 ± 6 Ma from this same complex obtained by Damm et al. (1986); as reported by Cortés et al. (2007). The Bólfin–Punta Tetas igneous complex is thus a relic of an Early Jurassic magmatic arc that has an extensive development in northern Chile, where it is mainly represented by the La Negra Formation volcanic rocks (e.g., Scheuber and Gonzàlez, 1999), which started to be erupted in the Sinemurian. This magmatic event was probably responsible for the Pb-loss shown by the metamict overgrowths in leucogranite MEJ-18029 and banded schist FO1139, and for 190–140 Ma cooling ages found throughout the Mejillones Peninsula (Basei et al., 1996; Diaz et al., 1985; Lucassen et al., 2000).

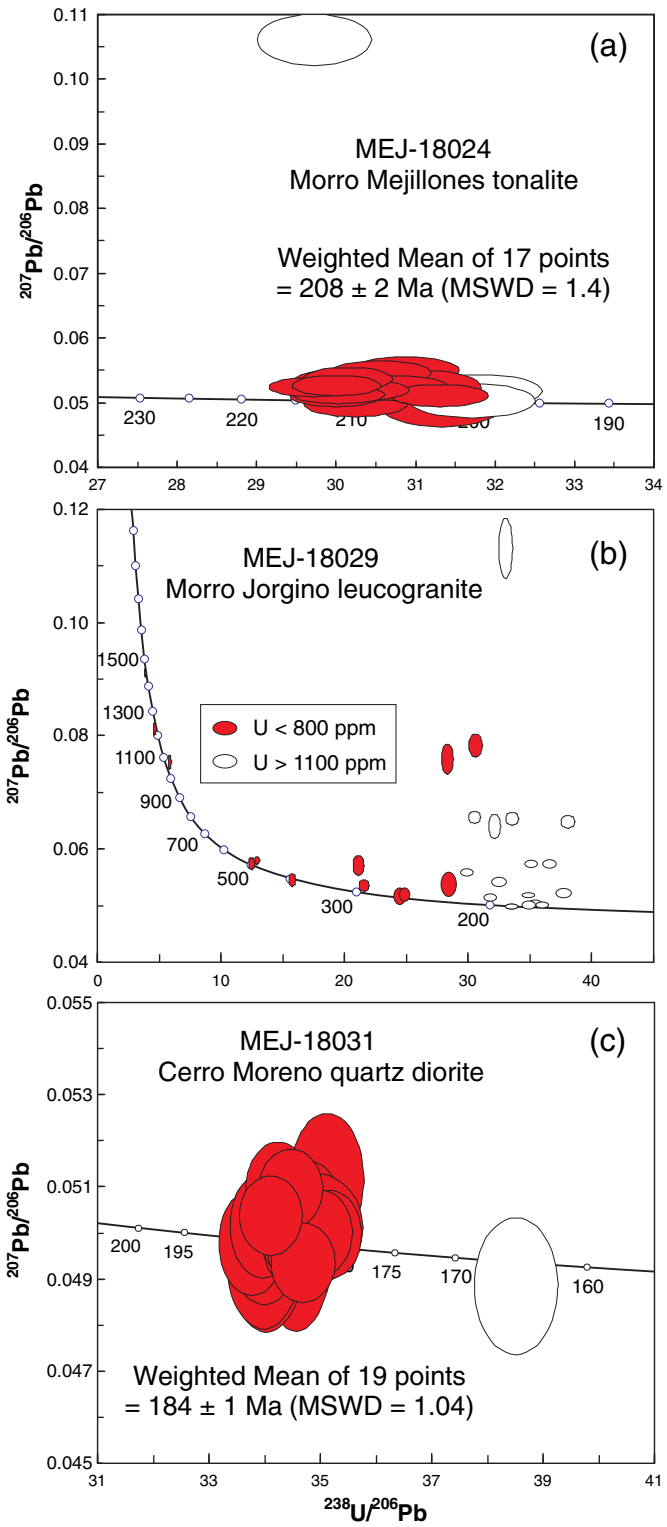

Fig. 5. Tera–Wasserburg plots of younger ages from zircons from the igneous rocks. Error ellipses are 68% confidence limits; white ellipses mark rejected points (in MEJ-18024 and MEJ-18031) and metamorphic rims (in MEJ-18029). NB. In accordance with the treatment of SHRIMP data in our previous publications and the original basis of this diagram (Tera and Wasserburg, 1972), the data are plotted without common-Pb correction so that deviation from the Concordia cannot be interpreted as discordance of the two U–Pb systems. The low count-rates for ^{204}Pb do not allow precise correction of $^{207}Pb/^{235}U$ ratios for low concentrations of ^{207}Pb, i.e., in young zircon with low-to-normal U contents; consequently our age estimates for zircon younger than ca. 800 Ma is based on common Pb corrections using the measured $^{238}U/^{206}Pb$ and $^{207}Pb/^{206}Pb$ ratio as in Williams (1998).

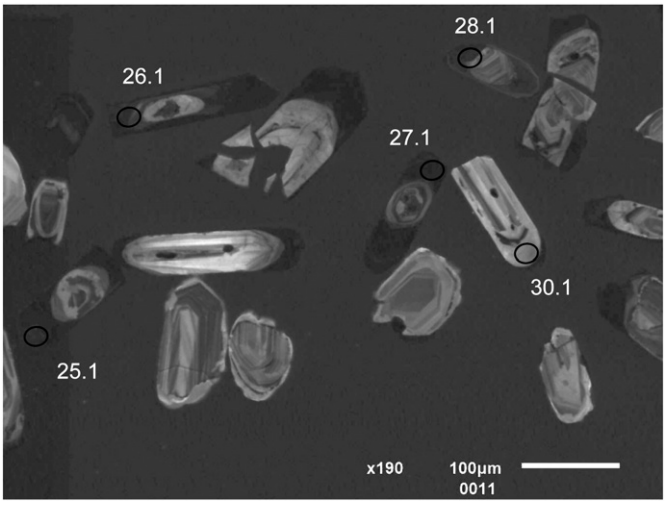

Fig. 6. CL image of MEJ-18029 showing grains exhibiting concentric igneous zonation, many of which have overgrowths with exceptionally high U contents (up to 8676 ppm), some of which are metamict.

Whether continuity existed between the Late Triassic magmatism (Morro Mejillones pluton) and the Bólfin–Punta Tetas Jurassic magmatic arc remains to be explored in more detail, as no intermediate ages have been recorded so far to our knowledge. However, evidence for annealing processes of Early Jurassic age recorded in the Late Triassic metamorphic and igneous rocks of Mejillones peninsula suggests that the latter were probably host to the Early Jurassic magmatic arc.

Remarkably, paleomagnetic data from Mejillones Peninsula indicates that no significant large scale latitudinal translation has taken place since the Jurassic (Hartley et al., 1992). The peninsula and the Bólfin area to the south were probably part of the same displaced block along the Atacama Fault system.

6. Conclusions

The Mejillones Peninsula is a composite block of Late Triassic (Norian) metamorphic and igneous rocks, and of Early Jurassic (Pliensbachian) plutons that reached its present position by displacement probably along the Atacama Fault system of northern Chile in the Jurassic and Early Cretaceous. Earlier suggestions of an Early Paleozoic metamorphism are not confirmed and are considered highly suspect.

The Mejillones metamorphic and igneous basement represents the end of the Late Permian to Late Triassic (Carnian) anorogenic cycle and the renewal of subduction and arc-magmatism along the pre-Andean continental margin in the Late Triassic (Norian). Relationships of this geodynamic event with the Early Jurassic Bólfin–Punta Tetas magmatic arc remain unknown.

Because the tectonostratigraphic evidence is markedly different on both sides of the Atacama fault system (e.g., Limón Verde) we suggest that the inferred status of Mejillonia as a transcurrent terrane (see Gibbons, 1994) be retained.

Acknowledgements

This research is a combined effort of projects CGL 2009-07984 (former Spanish Ministry of Science & Innovation); PIP CONICET 1940; BID 1728/OC AR PICT 1009 (Argentina) and FONDECYT 1095099 (Chile). A. Jensen (Universidad Catòlica del Norte) provided the geographical clues to identify the only road to access the top of Morro Jorgino block. Prof. Hans Massonne, Stuttgart University participated in one of the field trips. Juan Vargas (Universidad de Chile) separated the zircons. Carmen Galindo, Universidad Complutense, helped with

constructive comments and with the handling of figures. Mauricio Ibañez-Mejía and an anonymous referee are acknowledged for their helpful comments that helped to improve the manuscript.

References

Baeza, L., 1984. Petrography and Tectonics of the Plutonic and Metamorphic Complexes of Limon Verde and Mejillones Peninsula, Northern Chile. (Unpublished thesis) Eberhard Karls University Tübingen, Germany.

Bahlburg, H., Hervé, F., 1997. Geodynamic evolution and tectonostratigraphic terranes of northwestern Argentina and northern Chile. Bulletin of the Geological Society of America 109, 869–884.

Bahlburg, H., Vervoort, J.D., Du Frane, S.A., Bock, B., Augustsson, C., Reimann, C., 2009. Timing of crust formation and recycling in accretionary orogens: insights learned from the western margin of South America. Earth-Science Reviews 97, 215–241.

Basei, M.A.F., Charrier, R., Hervé, F., 1996. New ages (U–Pb, Rb–Sr, K–Ar) from supposed pre-Cambrian units in northern Chile: some geotectonic implications. Third International Symposium on Andean Geodynamics, pp. 763–766 (Saint Malo, France, Extended abstracts).

Brown, M., Diaz, F., Grocott, J., 1993. Displacement history of the Atacama fault system 25°00′ S–27°00′S, northern Chile. Geological Society of America Bulletin 105, 1165–1174.

Casquet, C., Rapela, C.W., Pankhurst, R.J., Baldo, E., Galindo, C., Fanning, C.M., Dahlquist, J., 2012. Fast sediment underplating and essentially coeval juvenile magmatism in the Ordovician margin of Gondwana, Western Sierras Pampeanas, Argentina. Gondwana Research 22, 664–673.

Cawood, P.A., Kröner, A., Windley, B., 2003. Accretionary orogens: definition, character, significance. European Geophysical Society. Geophysical Research Abstracts 5, 04856.

Cawood, P.A., Kröner, A., Collins, W.J., Kusky, T.M., Mooney, W.D., Windley, B.F., 2009. Accretionary orogens through Earth history. In: Cawood, P.A., Kröner, A. (Eds.), Earth Accretionary Systems in Space and Time: Geological Society of London, Special Publications, 318, pp. 1–36.

Charrier, R., Pinto, L., Rodriguez, M.P., 2007. Tectonostratigraphic evolution of the Andean Orogen in Chile. In: Moreno, T., Gibbons, W. (Eds.), The Geology of Chile. The Geological Society, London, pp. 21–114.

Cortés, J.C., Marquardt, C.R., González, G.L., Wilke, H-G.H., Marinovic, N., 2007. Carta Mejillones y Península Mejillones. Región de Antofagasta. Carta Geológica de Chile 1:100.000, SERNAGEOMIN, Santiago.

Cortés, J., Rémy, D., González, G., Martinod, J., Gabalda, G., 2008. Fractures in the Mejillones Península triggered by the Tocopilla Mw = 7.7 earthquake. 7th International Symposium on Andean Geodynamics (ISAG 2008, Nice), pp. 168–171 (Extended Abstracts).

Damm, K.W., Pichowiak, S., Todt, W., 1986. Geochemie, petrologie und geochronologie der plutonite un des metamorphen Grundgebirges in Nord-Chile. Berliner Geowissenschaftliche Abhandlungen, A/66, 73–146.

Damm, K.W., Pichowiak, S., Harmon, R.S., Todt, W., Kelley, S., Omarini, R., Niemeyer, H., 1990. Pre-Mesozoic evolution of the Central Andes, the basement revisited. Geological Society of America, Special Paper 241, 101–126.

Diaz, M., Cordani, U., Kawashita, K., Baeza, L., Venegas, R., Hervé, F., Munizaga, F., 1985. Preliminary radiometric ages from the Mejillones Peninsula, Northern Chile. In: Hervé, F., Munizaga, F. (Eds.), Evolución Magmática de los Andes. : Comunicaciones, 35. Departamento de Geología, Universidad de Chile, Santiago, pp. 59–67.

Ducea, M.H., Kidder, S., Chesley, J.T., Saleeby, J.B., 2009. Tectonic underplating of trench sedimentes beneath magmatic arcs: the central California example. International Geology Review 51, 1–26.

Gibbons, W., 1994. Suspect terranes. In: Hancock (Ed.), Continental Deformation. Pergamon Press, Oxford, pp. 305–319.

Hartley, A., Turner, P., Rex, D.C., Flint, S., 1992. Paleomagnetic, geochronological and geological constraints on the tectonic evolution of the Mejillones Peninsula, northern Chile. Geological Journal 27, 59–74.

Hartley, A.J., May, G., Chong, G., Turner, P., Kape, S.J., Jolley, E.J., 2000. Development of continental forearc: a Cenozoic example from the Central Andes, Northern Chile. Geology 28, 331–334.

Hervé, F., Mpodozis, C., 1990. Terrenos tectonoestratigráficos en la evolución geológica de los Andes chilenos: una revisión. Actas, XI Congreso Geológico Argentino, II. Asociación Geológica Argentina, San Juán, Argentina, pp. 319–323.

Hervé, F., Massonne, H.-J., Calderón, M., Soto, F., Fanning, C.M., 2010. Pre-Mesozoic metamorphism and tectonics in northern Chile: collisional vs. subduction zone environments. Eos, Transactions of the American Geohpysical Union 91 (26) (Meeting of the Americas Supplement, Abstract V11A-04).

Llambias, E.J., 1999. Las rocas ígneas gondwánicas. 1. El magmatismo gondwánico durante el Paleozoico Superior — Triásico. Geología Argentina: Anales del Instituto de Geología y Recursos Minerales, Buenos Aires, 29, pp. 349–363.

Lucassen, F., Becchio, R., Wilke, H.G., Franz, G., Thirlwall, M.F., Viramonte, J., Wemmer, K., 2000. Proterozoic–Paleozoic development of the basement of the Central Andes (18–26°). A mobile belt of the South American craton. Journal of South American Earth Sciences 13, 697–715.

Ludwig, K.R., 2001. SQUID 1.02. A user's manual: Berkeley Geochronological Center. Special Publication, 2, 2455 Ridge Road, Berkeley, Ca 94709, USA.

Matzel, J.E.P., Bowring, S.A., 2004. Protolith age of the Swakane Gneiss, North Cascades, Washington: evidence of rapid underthrusting of sediments beneath an arc. Tectonics 23, TC6009. http://dx.doi.org/10.1029/2003TC001577 (18 pp.).

Mezger, K., Krogstad, E.J., 2004. Interpretation of discordant U–Pb zircon ages: an evaluation. Journal of Metamorphic Geology 5, 127–140.

Niemeyer, H., González, G., Martínez-De los Rios, E., 1996. Evolución tectónica cenozoica del margen continental activo de Antofagasta, norte de Chile. Revista Geológica de Chile 23, 165–186.

Ramos, V.A., 1988. Late Proterozoic–Early Paleozoic of South America. A collisional history. Episodes 11, 168–174.

Rapela, C.W., Pankhurst, R.J., Casquet, C., Baldo, E., Saavedra, J., Galindo, C., Fanning, C.M., 1998. The Pampean orogeny of the southern Proto-Andes: a Cambrian continental collision. Evidence from the Sierras Pampenas de Cordoba (Argentina). Geological Society of London, Special Publications 142, 181–217.

Rocha-Campos, A.C., Basei, M.A., Nutman, A.P., Kleimann, L.E., Varela, R., Llambías, E., Canile, F.M., da Rosa, O. de C.R., 2011. 30 million years of Permian volcanism recorded in the Choiyoi igneous province (W Argentina) and their source for younger ash fall deposits in the Paraná Basin: SHRIMP U–Pb zircon geochronology evidence. Gondwana Research 19, 509–523.

Scheuber, E., Gonzàlez, G., 1999. Tectonics of the Jurassic–Early Cretaceous magmatic arc of the north Chilean Coastal Cordillera (22°–26° S): a story of crustal deformation along a convergent plate boundary. Tectonics 18, 895–910.

Stern, C.R., 2011. Subduction erosion: rates, mechanisms, and its role in arc magmatism and the evolution of the continental crust and mantle. Gondwana Research 20, 284–308.

Tera, F., Wasserburg, G., 1972. U–Th–Pb systematics in three Apollo 14 basalts and the problem of initial Pb in lunar rocks. Earth and Planetary Science Letters 14, 281–304.

Tomlinson, A.J., Blanco, N., García, M., Baeza, L., Alcota, H., Ladino, M., Pérez de Arce, C., Fanning, C.M., Martin, M.W., 2012. Permian Exhumation of Metamorphic Complexes in the Calama Area: Evidence for Flat-Slab Subduction in Northern Chile During the San Rafael Tectonic Phase and Origin of the Central Andean Gravity High. XIII Congreso Geológico Chileno, Antofagasta, Electronic Expanded Abstracts, thematic Session T2, pp. 209–211.

Williams, I.S., 1998. U–Th–Pb geochronology by ion microprobe. In: McKibben, M.A., Shanks III, W.C., Ridley, W.I. (Eds.), Applications of Microanalytical Techniques to Understanding Mineralizing Processes: Reviews of Economic Geology, 7, pp. 1–35.